HHS Public Access

Author manuscript

Glia. Author manuscript; available in PMC 2015 April 02.

Published in final edited form as:

Glia. 2012 December ; 60(12): 1839–1859. doi:10.1002/glia.22401.

Pro-inflammatory cytokine regulation of cyclic AMP-phosphodiesterase 4 signaling in microglia *in vitro* and following CNS injury

Mousumi Ghosh, Ph.D.[1], **Daniela Garcia-Castillo, B.S.**[1], **Vladimir Aguirre, B.S.**[1], **Roozbeh Golshani, Ph.D.**[1], **Coleen M. Atkins, Ph.D.**[1,2,4], **Helen M. Bramlett, Ph.D.**[1,2,4,7], **W. Dalton Dietrich, Ph.D.**[1,2,3,4,5,6], and **Damien D. Pearse, Ph.D.**[1,2,3,4,*]

[1]The Miami Project to Cure Paralysis, The University of Miami Miller School of Medicine, Miami, FL, 33185

[2]The Neuroscience Program, The University of Miami Miller School of Medicine, Miami, FL, 33185

[3]The Interdisciplinary Stem Cell Institute, The University of Miami Miller School of Medicine, Miami, FL, 33185

[4]Department of Neurological Surgery, The University of Miami Miller School of Medicine, Miami, FL, 33185

[5]Department of Neurology, The University of Miami Miller School of Medicine, Miami, FL, 33185

[6]Department of Cell Biology and Anatomy, The University of Miami Miller School of Medicine, Miami, FL, 33185

[7]Bruce W. Carter Department of Veteran Affairs Medical Center, Miami, FL, 33125

Abstract

Cyclic AMP suppresses immune cell activation and inflammation. The positive feedback loop of pro-inflammatory cytokine production and immune activation implies that cytokines may not only be regulated by cyclic AMP but conversely regulate cyclic AMP. This study examined the effects of TNF-α and IL-1β on cyclic AMP-phosphodiesterase (PDE) signaling in microglia *in vitro* and after spinal cord or traumatic brain injury (SCI, TBI). TNF-α or IL-1β stimulation produced a profound reduction (>90%) of cyclic AMP within EOC2 microglia from 30min that then recovered after IL-1β but remained suppressed with TNF-α through 24h. Cyclic AMP was also reduced in TNF-α-stimulated primary microglia, albeit to a lesser extent. Accompanying TNF-α-induced cyclic AMP reductions, but not IL-1β, was increased cyclic AMP-PDE activity. The role of PDE4 activity in cyclic AMP reductions was confirmed by using Rolipram. Examination of *pde4* mRNA revealed an immediate, persistent increase in *pde4b* with TNF-α; IL-1β increased all *pde4* mRNAs. Immunoblotting for PDE4 showed that both cytokines increased PDE4A1, but only TNF-α increased PDE4B2. Immunocytochemistry revealed PDE4B nuclear translocation with

*Address of Corresponding Author: Damien D. Pearse, The Miami Project to Cure Paralysis, University of Miami Miller School of Medicine, The Lois Pope Life Center, Locator code (R-48), PO BOX 016960, Miami, Florida, 33101, Phone 305 243 7139, Fax 305 243 3923, DPearse@miamiproject.med.miami.edu.

TNF-α but not IL-1β. Acutely after SCI/TBI, where cyclic AMP levels are reduced, PDE4B was localized to activated OX-42$^+$ microglia; PDE4B was absent in OX-42$^+$ cells in uninjured spinal cord/cortex or inactive microglia. Immunoblotting showed PDE4B2 up-regulation from 24h to 1wk post-SCI, the peak of microglia activation. These studies show that TNF-α and IL-1β differentially affect cyclic AMP-PDE signaling in microglia. Targeting PDE4B2 may be a putative therapeutic direction for reducing microglia activation in CNS injury and neurodegenerative diseases.

Keywords

cyclic AMP; phosphodiesterase; Rolipram; TNF-α; IL-1β; inflammation; CNS

Introduction

Central nervous system (CNS) injury induces an acute up-regulation of pro-inflammatory cytokines, including tumor necrosis factor (TNF)-α and interleukin-1β (IL-1β) (Streit et al., 1998; Yakovlev and Faden, 1994). These cytokines in turn initiate immune cell activation (Goodman et al., 2008; Pearse et al., 2004a) and play a central role in secondary neural damage (Pearse and Jarnagin, 2011), gliosis (Selmaj et al., 1991), and exacerbate neurological dysfunction. Although neurons and astrocytes have been reported to express pro-inflammatory cytokines (Breder et al., 1993; Sharif et al., 1993), activated microglia appear to be the predominant source in the CNS for a plethora of inflammatory mediators under pathological conditions (Lucin and Wyss-Coray, 2009), including TNF-α and IL-1β (Kita et al., 1997; Rice et al., 2007).

Microglial cell activation is a histopathological hallmark of CNS injury and neurodegenerative conditions. Pro-inflammatory cytokines released by injury-perturbed microglia are responsible for triggering a positive feedback loop of continual cytokine secretion and auto-activation (Pearse et al., 2004a). Although both IL-1β and TNF-α contribute to neuro-inflammation, these cytokines interact through structurally unrelated receptors (Baud and Karin, 2001; Wajant et al., 2003), exhibit differences in their downstream signaling pathways (Dunne and O'Neill, 2003), and display a temporal profile of expression following CNS injury that is disparate (Kinoshita et al., 2002; Vitarbo et al., 2004).

The ubiquitous cyclic adenosine monophosphate (cyclic AMP) pathway is one intracellular signaling cascade that prevents cellular reactivity and maintains homeostasis (Caggiano and Kraig, 1999). Addition of cyclic AMP analogs, adenylyl cyclase (AC) activators or phosphodiesterase (PDE) inhibitors, which elevate intracellular cyclic AMP levels, have been shown to retard microglia activation and antagonize pro-inflammatory cytokine production (Serezani et al., 2008). Although cyclic AMP signaling has been shown to regulate microglial cell reactivity and TNF-α and IL-1β production, it has not been demonstrated conversely how these pro-inflammatory cytokines can comparatively affect cyclic AMP signaling, a situation that occurs physiologically following CNS injury. Pro-inflammatory cytokines could decrease cyclic AMP levels and promote microglia activation

through two main effectors, a down-regulation of AC activity and/or an increase in PDE activity (Ma et al., 1999; Patrizio, 2004). Previously we have shown that following spinal cord injury (SCI) and traumatic brain injury (TBI) there is a profound, acute decrease in cyclic AMP levels that can be reversed by the PDE4 inhibitor, Rolipram (Atkins et al., 2007; Pearse et al., 2004b). This would imply that PDE4, which accounts for the majority of PDE activity in the CNS (Kleppisch, 2009), is the predominant PDE in immune cells (macrophages, eosinophils, neutrophils and microglia) (Semmler et al., 1993; Ghosh and Pearse, 2010) and has been identified in the injured spinal cord (Whitaker et al., 2008), could be regulated by pro-inflammatory cytokines such as TNF-α and IL-1β to decrease cyclic AMP. Rolipram, and other PDE4 inhibitors, in addition to preventing injury-induced decreases in cyclic AMP, also have potent anti-inflammatory actions (Bao et al., 2011; Atkins et al., 2007; Pearse et al., 2004b). Collectively this work implies that cyclic AMP dysregulation after CNS injury may be central to microglia activation and their ensuing auto-activation through pro-inflammatory cytokine production.

The objective of the current study was to examine how TNF-α and IL-1β temporally alter cyclic AMP levels and regulate PDE4 expression, protein production, sub-cellular localization and activity in microglia. The work in particular sought to determine whether these cytokines differentially affected cyclic AMP-PDE signaling based upon their distinct signaling pathways and whether changes induced by either TNF-α or IL-1β could be reversed by PDE4 inhibition. Lastly, the identification of which PDE4 gene products were expressed acutely after SCI and TBI in activated microglia was determined. This study provides a novel understanding of the molecular mechanisms involved in pro-inflammatory cytokine regulation of microglial cell activation and offers a putative therapeutic direction for targeting inflammation in CNS injury and neurodegenerative diseases.

Materials and Methods

Cell Culture and Viral Vectors

EOC2 Microglia Culture—The immortalized murine microglia cell line, EOC2 (CRL-2467, purchased from ATCC, Manassas, VA) was employed for these studies as they exhibit both phenotypical and functional properties of primary microglial cells (Walker et al., 1995). Microglia were cultured at 37°C, 5% CO_2 in Dulbecco's modified Eagle's medium supplemented with 10% heat-inactivated fetal bovine serum (HyClone, Logan, UT), 20% Ladmac conditioned media (ATCC), 100 units/ml penicillin and 100 μg/ml streptomycin (Sigma-Aldrich, St. Louis, MO). For pro-inflammatory cytokine stimulation experiments, microglia were seeded on either 100 mm or 60 mm culture dishes (1×10^6 or 5×10^5 cells/dish, respectively; for biochemistry) or 4-well chamber slides (5×10^5 cells/well; for immunocytochemistry) and grown to 60–70% confluence. Cytokine stimulation involved the addition of either TNF-α (10ng/ml; R&D, Billerica, MA) or IL-1β (5ng/ml; R&D), with/without Rolipram (10 μm, Sigma), for time intervals between 0 to 24h. These concentrations have been used in previous *in vitro* studies of microglial cell activation (Pearse et al., 2004a) and are similar to the tissue levels seen following CNS trauma, which have been measured at 1–10ng/ml (Bethea et al., 1999). Cytokines were added in 1μl water while Rolipram was used in 1μl of 100% Dimethyl sulfoxide (DMSO); the amounts of these agents were based

upon the final desired concentrations in culture as described above. Water or DMSO was used as a vehicle-only in untreated, control cultures; DMSO was found not to affect microglial activation when given alone as such a dilute concentration. Except for the time course studies of cyclic AMP and PDE4 activity/mRNA changes in which 5 time points were examined (0, 0.5, 3, 12 and 24h post-stimulation were examined), all other work employed an endpoint period of 3 and/or 24h after cytokine exposure, time points in which protein changes would be expected (3h) or at which microglia cells have undergone a complete morphological change to an activated phenotype (24h).

Primary Microglia Culture—Primary microglial cells were collected from the dissociated cerebral cortex of adult Fisher rats according to procedures by Mecha et. al., (2011); modifications were made to permit the isolation of purified microglia (>90%) from adult rather than postnatal rats. Briefly, the cortical lobes were dissected and cut into 2mm pieces to allow easy trituration. The tissue was suspended in cold DMEM (Dulbecco's Modified Eagle Medium, Gibco, Life Technologies Corporation) and triturated using a P-1000 plastic tip. The cell suspension was passed through a 100 μm cell strainer followed by centrifugation at X1000 rpm for 10min. The supernatant was removed and the pellet re-suspended in DMEM containing 10% FBS and 10% horse serum (Gibco, Life Technologies Corporation). The cell suspension was plated on polylysine coated T75 flasks and incubated at 37°C for 7 to 10 days. Thereafter, cultures were placed on an orbital shaker at X230 rpm for 3 hours. The cell suspension, containing the microglial cell population, was taken for centrifugation for 10min at X1000 rpm to obtain the microglial cell fraction in the pellet. The pellet was collected, resuspended in the same media as above and the number of viable cells was determined using Trypan Blue followed by quantification using a Neubauer's chamber. An average yield of ~5×10^5 cells was obtained per rat brain. The cell suspension was diluted to the desired cell concentration and plated for at least 24h for use in *in vitro* experiments according to the same experimental schema as described for the EOC2 microglial cell line.

Lentiviral Vectors—A replication incompetent Lentiviral Vector (LV) encoding a *pde4b* short hairpin RNA (shRNA) was obtained from Santa Cruz Biotechnology Inc. (Cat. No. sc-44003-V) as a pool of concentrated, transduction-ready viral particles composed of three target-specific constructs that encoded a 19–25 nucleotide (plus hairpin) shRNA designed to knock down gene expression of *pde4b* isoforms.

Animals

TBI was performed using 4 adult male Sprague Dawley rats (300–400g, Charles Rivers Laboratories, Wilmington, MA; 2 sham and 2 injured animals), while for SCI, 73 adult female Fischer rats (180–200g, Harlan Laboratories, Indianapolis, IN; 12 uninjured and 61 injured animals) were used. All experimental procedures were performed in compliance with the National Institute of Health Guide for the Care and Use of Laboratory Animals and approved by the University of Miami Institutional Animal Care and Use Committee.

Spinal Cord Contusion Injury Model—Contusion injury was induced by the MASCIS weight drop device developed at New York University (Gruner, 1992). Prior to surgical

procedures, animals were weighed and anesthetized by i.p. injection (45mg/kg ketamine, 5mg/kg xylazine). An adequate level of anesthesia was determined by monitoring the corneal and hind limb withdrawal reflexes. Animals were prepared pre-operatively as described previously (Ghosh et al., 2012). A laminectomy performed at thoracic vertebra T8 exposed the dorsal surface of the spinal cord underneath (T9) without disrupting the dura mater. The exposed spinal cord was moderately injured by dropping a 10.0g rod from a height of 25.0mm. The contusion impact height, velocity and compression were monitored. Animals (n=3) were excluded immediately when height or velocity errors exceeded 7% or if the compression distance was not within the range of 1.75 to 2.25mm. After injury, the muscles were sutured in layers and the skin closed with metal wound clips. The rats were allowed to recover in a warmed cage with water and food easily accessible. Post-operative care was then administered as described in Patel et al. (2010).

Fluid-percussion Brain Injury Model—Fluid-percussion TBI was performed as described previously (Atkins et al., 2007). Briefly, animals were anesthetized with 3% isoflurane, 70% N_2O, and 30% O_2. The animals received a 4.8mm craniotomy (3.8mm posterior to bregma, 2.5mm lateral to midline) over the right parietal cortex and a beveled plastic 18 gauge syringe hub was secured to the craniotomy with cyanoacrylate and dental cement. At 24h after recovery from the craniotomy, the animals were re-anesthetized, intubated, and mechanically ventilated (Stoelting, Wood Dale, IL, USA) with 0.5% isoflurane, 70% N_2O, and 30% O_2. Pancuronium bromide (1.0mg/kg) was administered through the tail artery to immobilize the rats. A moderate (2.0±0.2atm) fluid-percussion pulse (22ms duration) was delivered to the right parietal cortex. Sham-operated rats received all of the surgical manipulations, with the exception of the fluid-percussion pulse. Physiological monitoring and post-operative care was performed as described elsewhere (Atkins et al., 2007).

Animal Perfusion and Tissue Extraction—For animal perfusion, at 24h after SCI or TBI, rats were deeply anesthetized [SCI, 70mg/kg ketamine, 10mg/kg xylazine; TBI, 3% isoflurane and 70% N_2O] and transcardially perfused, first with physiological saline [SCI, 200ml; TBI, 2 min, 4°C, 75ml) and then with ice-cold phosphate-buffered 4% paraformaldehyde (0.1M, pH 7.4; SCI, 500ml; TBI, 350ml); extracted CNS tissue underwent post-fixation and cryoprotection as described elsewhere (Schaal et al., 2007). The T7-T11 thoracic spinal cord (20-mm-long piece) or the brain (10mm length from BR +2.00 to −8.00), which contained the injury site, was dissected. The spinal cords were embedded in Tissue-Tek for cryosectioning at 40μm (saggital) on a Leica CM3050S Cryostat (Leica Microsystems Inc., Buffalo Grove, IL). The brains were sectioned in PBS (50 μm thick, coronal) with a Leica vibratome (Leica Microsystems, Inc., Exton, PA). Every sixth section was collected (for 6 series in buffer; PB 0.1M pH 7.4, 0.1% NaN_3) and stored at 4°C until further processing. For mRNA and protein analysis by Q-PCR and western blotting, respectively, animals were deeply anesthetized at endpoint as above and 5-mm pieces of spinal cord encompassing the injury/graft site was taken, snap frozen at −80°C in liquid nitrogen and stored in liquid nitrogen until further processing.

Molecular Biology

RNA isolation and quantitative PCR analysis (qPCR)—Quantitative Real Time Polymerase Chain Reaction (qPCR) was used to quantify mRNA expression of different *pde4* genes in cytokine-activated and naïve control microglia temporally (0, 30min, 1h, 3h, 12h and 24h) grown on 100mm dishes or from spinal cords (T7-9; 5mm piece) from animals uninjured or temporally post-SCI (0, 2h, 24h, 3d, 1wk, 2wk, 4wk and 8wk). Following isolation of total RNA using Trizol (Invitrogen, Carlsbad, CA), cell lysates or tissue homogenates were treated with DNAse (Invitrogen) and the reaction terminated by heating at 65°C for 10min. To permit mRNA analysis, 2μg of total RNA was reverse-transcribed into cDNA using the Bio-Rad first-strand cDNA synthesis kit as per manufacturer's instructions (Biorad, Hercules, CA). After chloroform (200μl) addition, samples were centrifuged and the aqueous layer transferred to a fresh tube. Isopropanol (600μl) was then added, followed by centrifugation to pellet the RNA and a 75% ethanol rinse. Samples were resuspended in 100μl RNase-free H_20 and treated with a RNA clean-up kit (SABiosciences, Frederick, MD) for subsequent qPCR. The concentration and purity of RNA were determined using a Nanodrop spectrophotometer (ThermoFisher Scientific, Pittsburgh, PA) at 260/280 nm. The qPCR was carried out in 96-well plates for each of the samples in triplicates using the Eppendorf Mastercycler EP Realplex System (Eppendorf, Westbury, NY). The mRNA levels for each target *pde4* gene was quantified by SYBR Green-based qPCR using the QuantiTect SYBR Green PCR kit (Qiagen Inc, Valencia CA) according to manufacturer's instructions using specific custom primers against the different *pde4* gene products. The primers used were: *pde4a*: 5′-tcaaaggtcaaaggccagag-3′, 5′-tttcaaggctgaaggaatgg-3′; *pde4b*: 5′-atgataccccagagcccttc-3′, 5′-gccttctccctcctttttcc-3′; *pde4d*: 5′-agtggtaccagagcacaatcc-3′, 5′-cttcctccacctgacttcca-3′; and as a control, *gapdh*: 5′-atggccttccgtgttcctac-3′, 5′-gcctgcttcaccaccttct-3′. Melting curve analysis confirmed the specificity of each reaction. The reaction was performed using 5μl of cDNA, 0.25–0.5μM of primer, and 2x SYBR Green Super Mix (Qiagen) with a final volume of 25μL. Quantification was performed using the standard curve method. Values of the relative amount of gene expression for specific *pde4* mRNA were normalized to the transcript amounts of the constitutively expressed gene, glyceraldehyde-3-phosphate dehydrogenase (*gapdh*), which served as an internal standard. The relative expression levels of target *pde4* mRNA was calculated from the measured threshold cycles (Ct) by a standard curve.

Biochemistry

Western Blot Analysis—Immunoblotting was used to quantify protein production of different PDE4 isozymes in cytokine-activated and naïve control microglia temporally (0, 30min, 1h, 3h, 12h and 24h) grown on 100mm dishes or tissue homogenates obtained from spinal cords (T7-9; 5mm piece) from animals uninjured or temporally post-SCI (24h, 3d, 1wk, 2wk and 4wk) according to previously published methods (Pearse et al., 2001). Briefly, microglia were treated with ice-cold lysis buffer: 15mM Tris pH 7.6, 0.25M sucrose, 1mM $MgCl_2$, 1mM EGTA, 1mM DTT, 1.25μg/ml pepstatin A, 10μg/ml leupeptin, 25μg/ml aprotinin, 1mM benzamidine, 0.5mM PMSF, 1mM Na_3VO_4, 50mM NaF, 2mM $Na_4P_2O_7$, and 1X Complete Mini Roche cocktail protease inhibitor (Roche, Indianapolis, IN). Next, lysates were assayed for total protein concentration using the Coomassie Plus

protein assay (Bio-Rad Laboratories, Hercules, CA). The extracted samples were boiled with 1X SDS sample buffer for 10min at 100°C. Then equal amounts of protein (30μg/lane) from each sample underwent gel electrophoresis (10% SDS-PAGE) and were transferred to Polyvinylidene fluoride (PVDF) membranes. PVDF membranes were blocked with 3% BSA in Tris buffered saline with 0.1% Tween (TBST; 50mM Tris HCl, pH 7.4, 150mM NaCl and 0.1% Tween), then probed with pan-PDE4-specific primary antibodies. The primary antibodies used were rabbit anti-PDE4A, anti-PDE4B and anti-PDE4D (1:500, Santa Cruz Biotechnology Inc., Santa Cruz, CA), anti-PDE4B2 (1:1,000, EMD Millipore, Billerica, MA) and mouse anti-β-actin (1:10,000, Sigma-Aldrich). These pan-PDE4 antibodies recognize all spliced variants of the specific PDE4 gene product, A, B or D. Identification of specific PDE4 spliced variants was made based upon known molecular weights. Specific bands were visualized with HRP-conjugated secondary antibodies (1:5,000, Jackson ImmunoResearch Laboratories, Inc., West Grove, PA) using a chemiluminescence detection kit, Supersignal West PICO (Pierce, Rockford, IL) and developed on film (GeneMate, Blue basic Autorad Film, Bioexpress, UT). The optical density of the bands (arbitrary units) was measured with an imaging Densitometer (Bio-Rad) and levels of each of the PDE4 bands were normalized to β-actin within each sample run in the same gel.

Cyclic AMP Assay—The cyclic AMP assay was used to measure changes in cyclic AMP levels in cytokine-activated and naïve control microglia temporally (0, 30min, 1h, 3h, 12h and 24h) grown on 60mm dishes. Microglial cell cultures were lysed by the addition of 1X cell lysis buffer (Cell Signaling Technology Inc., Danvers, MA), containing IBMX (0.5mM; Tocris, Ellisville, MI) and Rolipram (100μM; Sigma), and incubated for 30min on ice. The total cell lysates were centrifuged for 10min at 1,000 × g at 4°C. Protein concentrations were determined using the Bio-Rad modified Bradford protein assay with BSA as standard (Bio-Rad Laboratories). Supernatants were analyzed for total cyclic AMP levels using a cyclic AMP detection kit (cyclic AMP-Glo™ Assay; Promega Corporation, Madison, WI) as per manufacturer's instructions. Levels of cyclic AMP were expressed as a percentage of the naïve control.

Phosphodiesterase Activity—Levels of cyclic AMP-specific PDE activity were measured in cytokine-activated and naïve control microglia temporally (0, 30min, 1h, 3h, 12h and 24h) grown on 60mm dishes. Microglial cell cultures were lysed by the addition of 1X cell lysis buffer (Cell Signaling Technology Inc.) containing cocktail protease inhibitors (Roche) and total protein concentration estimated using the Bio-Rad modified Bradford protein assay with BSA as standard (Bio-Rad Laboratories). Lysates were assayed for total cyclic AMP-PDE activity using a cyclic AMP-PDE-specific PDE-Glo ELISA kit (Promega Corporation). A final concentration of 25μg protein was used per assay with each assay carried out in triplicate as per the manufacturer's instructions. The enzymatic reaction was performed using cyclic AMP as a substrate (1mM final concentration) in the presence of enzyme inhibitors or the enzyme alone. The reaction mixture was incubated at 25°C for 30min and then stopped by the addition of PDE-Glo™ Termination Buffer containing IBMX at a final concentration of 0.5mM. As a negative control, heat-inactivated, total microglial cell lysates were incubated in the above-mentioned buffer at 30°C for 15min and

then 1mM of cyclic AMP was added. Total cyclic AMP-PDE specific activity was obtained in pmoles/min/mg protein.

Immunocytochemistry—For immunofluorescence microscopy, cytokine-treated or naïve control microglial cells were grown on 4-well glass chamber slides (Lab-Tek Inc., Grand Rapids, MI) and fixed at specific time points post-stimulation with 4% paraformaldehyde in 0.1M PBS. Fixed cells were then rinsed using 1X PBS, permeabilized with 0.1% Triton-X 100 for 5min at 37°C, and then incubated with 2% BSA in PBS for 1h to block non-specific binding. Primary anti-pan-PDE4 antibodies (as described for immunoblotting) were added for 2h at 25°C, followed by 3X washes with PBS. The cell morphology was demarcated using a fluorescent-conjugated antibody against actin, Phalloidin-488 (1:200, Life Technologies Corporation, Grand Island, NY). To confirm cellular localization of the PDE4B2 splice variant, a PDE4B2-specific antibody (1:100, EMD Millipore) was used for immunohistochemistry according to the protocol above. In addition to immunohistochemistry for PDE4s, specific antibodies recognizing cyclic AMP (1:200, Abcam, Cambridge, MA) and TNF-α (1:200, MyBioSource, LLC San Diego, CA), macrosialin (mouse anti rat CD68/ED1, 1:200, AbD Serotec, Raleigh, NC), a lysosomal protein expressed on activated, mononuclear phagocytes (Damoiseaux et al., 1994; Pearse et al., 2004a) and CD11b (OX-42, 1:100, AbD Serotec), also highly expressed on activated, mononuclear phagocytes, were also employed using the aforementioned methodology. Specific protein localization was detected by incubation for 1h with Alexa-594 or Alexa-488 conjugated goat anti-rabbit secondary antibodies (Life Technologies Corporation). Incubation with Hoechst 33342 for 10 min (1:1000; Life Technologies Corporation) permitted labeling of cell nuclei. Immunostained slides were coverslipped with Vectashield mounting medium (Vector Laboratories, Burlingame, CA) and kept protected from light at 4°C until observation to avoid photo-bleaching. The localization of PDE4 protein in samples was imaged and assessed in at least three random fields per slide using a LSM510 confocal laser-scanning microscope (Carl Zeiss, Jena, Germany).

Immunohistochemistry—Free-floating, coronal brain sections (50μm-thick; Bregma -4.2mm) or saggital spinal cord sections (40μm-thick; at the injury epicenter) were used for immunohistochemical localization of PDE4 proteins in activated microglia after sham surgery or SCI/TBI by previously described methods (Barakat et al., 2005). Primary anti-PDE4 antibodies (as described for immunoblotting) and mouse anti-OX-42 (1:200; Wako, Richmond, VA) were used. For visualization, the secondary antibodies, goat anti-mouse Alexa-488 and anti-rabbit Alexa-594 (Invitrogen) were employed as well as Hoechst 33342 (1:500; dilution, Invitrogen, Eugene, OR) to detect cell nuclei. Specific PDE4 staining was confirmed using secondary or primary antibody only controls. Sections were mounted onto Snowcoat X-tra slides (Surgipath, Richmond, IL) and coverslipped with Vectashield mounting medium (Vector Laboratories, Burlingame, CA).

Flow Cytometry—A 5mm piece of the injured spinal cord was extracted 3d post injury into RPMI medium + 10% FCS. The tissue was immediately placed on a 70μm nylon cell strainer and was homogenized through the strainer using the black rubber surface of a 1ml syringe. After 3X rinses with HBSS, a single cell suspension was obtained, which was then

transferred to FACS tubes and centrifuged at 1,400 rpm for 5min at 4°C. The supernatant was removed and replaced with 1ml of FACS buffer (HBSS containing 2% FCS and 0.1% NaN_3) and the pellet re-suspended to obtain a uniform suspension. The cell suspension was then fixed using 2% paraformaldehyde in 0.1M PBS on ice for 15min followed by 2X washes with PBS. The cells were counted and 2×10^6 cells were used for flow cytometry analysis with each set of markers. For immunostaining, the cells were first permeabilized for 5min using 0.1% Triton X100 in PBS followed by blocking through incubation with 5% heat-inactivated goat serum for 30min at room temperature. Thereafter, anti-rabbit PDE4A or PDE4B polyclonal antibody (1:200, Santa Cruz Biotechnology) and anti-mouse OX-42 monoclonal antibody (1:200, Wako, Richmond, VA) was added to the cell suspension for 2h incubation at room temperature. Cells were washed with staining buffer and incubated in secondary antibody conjugated with goat anti-rabbit Alexa-594 and goat anti-mouse Alexa-488 (Invitrogen) for 1h at room temperature (in the dark). Cells were next washed 3X with FACS buffer and finally suspended in 300μl staining buffer. Flow cytometry acquisition was carried out using FITC and APC channels on the Becton Dickinson (BD) FACS Calibur Flow Cytometric Analyzer. The Mean Value of Fluorescence was obtained from the gating of 10,000 cells.

Imaging

Confocal Microscopy and Image Analysis—Images were acquired by sequential scanning of the immunostained cells or tissue sections with an Olympus Fluorescence microscope (Olympus, Fluoview FV 1000) or a confocal laser-scanning microscope (Carl Zeiss, LSM 500) at laser lines of 405, 488 and 594 nm. For presented images, the tonal range and sharpness (smart sharpen, 0.9 pixels) of the Tiff files were normalized using Adobe Photoshop CS2 (Adobe Systems Inc., San Jose, CA).

Statistics

Statistical significance was determined by performing a one-way analysis of variance (ANOVA) followed by Bonferroni test. Differences were considered significant at $*p< 0.05$. All errors are given as the SEM.

Results

EOC2 Microglia treated with either TNF-α and IL-1β exhibited a characteristic pattern of morphological and immunophenotypical activation

Naïve EOC2 microglia exhibited a stellate morphology characteristic of resting CNS microglia and rarely expressed the lysosomal protein macrosialin (ED1; Figure 1A–C), which is present only in activated cells of the monocytic lineage. Within 24h of stimulation with either TNF-α (Figure 1D–F) or IL-1β (Figure 1G–I), the morphology of the microglial cells changed to a rounded phenotype and robust immunoreactivity for ED1 was observed. No definitive difference in morphology or ED1 staining was observed between TNF-α and IL-1β activated microglia.

TNF-α and IL-1β dramatically reduced cyclic AMP levels in EOC2 microglia, though their regulation of cyclic AMP was disparate

In microglia exposed to either TNF-α or IL-1β, a pronounced reduction in cyclic AMP levels was observed within 30min of stimulation (TNF-α, decrease to 3.4±2.0% of untreated; IL-1β, decrease to 0.5±0.2% of untreated; Figure 2). While a biphasic recovery of cyclic AMP was observed at 1h (71.9±23.5%) and 12h (24.2±15.0%) following IL-1β compared to untreated controls, TNF-α induced a persistent reduction in cyclic AMP through 24h post-stimulation. At 24h after cytokine challenge, cyclic AMP levels were at 7.5±5.3% and 1.1±0.3% of untreated controls, respectively, for TNF-α and IL-1β treated microglia (Figure 2).

Expression of *pde4a*, *b* and *d* mRNA was increased by IL-1β, but only *pde4b* was elevated by TNF-α in EOC2 microglia

The expression of mRNA for *pde4a*, *b* and *d* was measured in naïve and cytokine challenged microglia from 30min to 24h (Figure 3). Expression of *pde4a* remained largely unchanged or slightly decreased (0.4-fold reduction at 3h) in microglia following TNF-α stimulation (Figure 3A). A pronounced and persistent increase in *pde4a* mRNA, however, was observed with IL-1β, with a 2.4–fold increase in expression at 30min, a 3.1–fold increase at 12h and elevated expression still present at 24h. Significant, transient increases in *pde4b* expression were observed with both TNF-α and IL-1β stimulation in microglia, though the temporal timing of this change differed between cytokines (Figure 3B). While an increase in *pde4b* mRNA was observed with IL-1β within 30min of stimulation (3.7-fold increase), peaking at 1h (4.5-fold increase), TNF-α induced increases in *pde4b* were not seen until 1h post-stimulation (5.1-fold increase) and *pde4b* mRNA levels remained elevated through 12h (1.8-fold increase). TNF-α failed to increase expression of *pde4d* mRNA in microglia, instead a significant reduction in *pde4d* mRNA from 3 to 24h post-stimulation was observed (24h, 0.5-fold decrease; Figure 3C). Biphasic, transient increases in *pde4d* expression occurred in microglia in response to IL-1β stimulation at 30min (2-fold increase) and 12h (2.6-fold increase; Figure 3C).

Both TNF-α and IL-1β stimulation enhanced production of PDE4A1, while TNF-α also induced a strong production of PDE4B2 in EOC2 microglia

Very low basal production or undetectable amounts of PDE4A, B and D were observed in naïve microglia (Figure 4). At 24h after challenge with TNF-α or IL-1β (Figure 4B–C), significant PDE4A immunoreactivity was observed in the cytoplasm of phalloidin-488-labeled microglia, being significantly more pronounced in those treated with TNF-α. Similarly, increased PDE4B immunoreactivity within the cytoplasm of microglia was observed at 24h after cytokine stimulation (Figure 4D–F). Like PDE4A, PDE4B immunoreactivity was significantly greater following TNF-α exposure. No observable changes in PDE4D immunoreactivity in microglia was observed among experimental conditions (Figure 4G–I).

Western blot analysis of cell lysates obtained from TNF-α-stimulated microglia showed significant increases in the short isoforms of PDE4A and B, PDE4A1 and PDE4B2, with molecular weights of 66 and 68kDa, respectively (Figure 5A–B). PDE4A1 exhibited a

significant increase from 30min to 12h (30 min, 87.0% increase; 24 h, 94.4% increase) after TNF-α-stimulation (Figure 5A), while PDE4B2 was significantly elevated at 30min (76.7% increase) and continued to gradually increase through 24h (206.7% increase; Figure 5B). IL-1β also increased PDE4A1 in microglia, from 1 to 12h post-stimulation (1h, 56.5% increase; 12h, 40.6% increase; Figure 5C), though no change in PDE4B2 was observed (Figure 5D). Longer isoforms of PDE4A and B as well as PDE4D were not detected in naïve or cytokine stimulated microglia with the antibodies employed.

TNF-α and IL-1β induced a different subcellular localization of PDE4B in activated EOC2 microglia

While PDE4A was localized to the cytoplasm under naïve conditions and following TNF-α and IL-1β stimulation, PDE4B exhibited a disparate subcellular localization among the two pro-inflammatory cytokines (Figure 6). In TNF-α-treated microglia, PDE4B was almost exclusively localized to the nucleus at 3h (and up to 12h) after stimulation (Figure 6A–C). In contrast, at 3h, PDE4B was localized predominantly to the cytoplasm after IL-1β exposure (Figure 6D–F). Subcellular localization of PDE4B in the nucleus of microglia after TNF-α (Figure 6G–H) and the cytoplasm following IL-1β (Figure 6I–J) was confirmed by histogram analysis of a 0.5μm cell slice under confocal microscopy.

PDE4B2 contains a putative nuclear localization sequence (NLS)

Bioinformatics analysis using PredictNLS (http://www.predictprotein.org) was performed on PDE4B, cyclic AMP-specific (Mus musculus; GenBank: CAM26138.1) sequence as shown in the Supplemental Materials section. A potential NLS shown in red (DREKKKK) was detected in this sequence, which exhibited an amino acid sequence similarity to the generalized NLS sequence of [DE]RxKKKK that has been found to occur in 15 other nuclear proteins of eukaryotic origin. Analysis of PDE4B isoforms from Homo sapiens (ACCESSION NP_002591) and Rattus norvegicus (ACCESSION NP_058727) also revealed this putative NLS sequence and showed it to be highly conserved across species.

TNF-α and IL-1β up-regulated cyclic AMP-dependent PDE activity in EOC2 microglia

We measured total cyclic AMP-dependent PDE activity in lysates from microglia challenged with TNF-α or IL-1β (Figure 7). TNF-α exposure resulted in a rapid, significant increase in cyclic AMP-PDE activity over naïve controls within 30min (2.7-fold) that remained elevated, and even substantially increased, by 24h (7.3-fold). In contrast, cyclic AMP-PDE activity changes with IL-1β were transient, significantly increasing only at 12h post-stimulation (2.9-fold).

Rolipram inhibited TNF-α-induced reductions in cyclic AMP levels and abrogated PDE4 induction in activated EOC2 microglia

To address the involvement of PDE4 in the dramatic reductions of cyclic AMP levels within microglia by TNF-α and IL-1β we employed the PDE4 inhibitor Rolipram (Figures 8 and 9). The 3h post-stimulation period was chosen for this investigation due to the pronounced reductions in cyclic AMP that occurred under both conditions at this time. In naïve microglia, immunocytochemistry revealed high levels of cytoplasmic cyclic AMP, modest

immunoreactivity for TNF-α and very low amounts of PDE4A and B staining (Figure 8A–D, 9A–D). At 3h after TNF-α exposure, the level of cyclic AMP immunostaining was significantly reduced (54% reduction, 8E), TNF-α immunoreactivity was pronounced (3.4-fold elevation over untreated controls, 8F) and both PDE4A (8G) and PDE4B (8H) immunoreactivity was significantly increased (6.1-fold and 26.2-fold, respectively) with proteins localized to the cytoplasm or nucleus, respectively. The simultaneous addition of Rolipram with TNF-α completely reversed its effects on cyclic AMP (8I), reduced the amount of TNF-α and PDE4A immunoreactivity to levels comparable to that of naïve controls (8J and 8K, respectively) and partially abated increases in PDE4B immunostaining (8L). Similar to TNF-α, IL-1β exposure dramatically reduced cyclic AMP staining (46.7% reduction, 9E) and increased levels of TNF-α (2.8-fold increase, 9F), PDE4A (1.7-fold increase, 9G) and B (9.4-fold increase, 9H), though the changes in TNF-α and PDE4 immunoreactivity were less pronounced than that seen with TNF-α exposure. The use of Rolipram during IL-1β stimulation recovered cyclic AMP to levels significantly higher (20%) than untreated controls (9I), diminished TNF-α immunoreactivity (9J), abrogated PDE4A staining (9K) and reduced PDE4B (9L) to levels comparable to that of naïve controls.

Knockdown of *pde4b* in microglia prevented TNF-α-induced reductions in cyclic AMP levels in activated EOC2 microglia

To investigate the role of PDE4B in mediating cyclic AMP changes in response to TNF-α, specific PDE4B knockdown was achieved using lentiviral vector mediated *pde4b* shRNA infection of microglia (LV-*pde4b*-shRNA; Figure 10). At 48h after infection of microglia with LV-*pde4b*-shRNA and 1h of TNF-α stimulation, the cytokine-induced increase in PDE4B was dose-dependently (based upon the LV multiplicity of infection, MOI) reduced by up to 77.6% (MOI 60; Figure 10A). Investigation of cyclic AMP levels in the same paradigm demonstrated that LV-*pde4b*-shRNA at a MOI of 10 effectively abated TNF-α induced reductions and when employed at a greater MOI, of 60, significantly increased cyclic AMP levels (2-fold) above that of the naïve microglia controls (Figure 10B).

Cyclic AMP levels are significantly reduced in primary microglia upon exposure to TNF-α or IL-1β

In primary microglia exposed to either TNF-α or IL-1β, a significant reduction in levels of cyclic AMP was observed at 24h after stimulation (TNF-α, decrease to 70.2±7.2% of untreated; IL-1β, decrease to 80.0±2.9% of untreated; Figure 11). The lysosomal marker ED1 was used for identification of activated microglia (Damoiseaux et al., 1994; Pearse et al., 2004a); untreated primary microglia controls exhibited pronounced ED1 immunoreactivity, which is indicative of the induction of cell reactivity that is known to occur during tissue harvesting and cell isolation (Hurley et al., 1999; Pearse et al., 2004a).

TNF-α and IL-1β stimulation enhanced production of TNF-α, PDE4A and PDEB, specifically PDE4B2, in primary microglia

Immunocytochemical staining for TNF-α and PDE4 gene products in primary microglia showed the presence of TNF-α, PDE4A, PDE4B and the spliced variant, PDE4B2 (Figure

12). At 24h after challenge with TNF-α or IL-1β, significant increases in TNF-α (TNF-α, increased 217%; IL-1β, increased 146%; Figure 12A–C), PDE4A (TNF-α, increased 169%; IL-1β, increased 147%; Figure 12E–G) and PDE4B (TNF-α, increased 170%; IL-1β, increased 143%; Figure 12I–K) were observed in $ED1^+$ microglia. Similarly, the PDE4B spliced variant, PDE4B2, exhibited 226% and 211% increases in immunoreactivity at 24h after TNF-α or IL-β1 exposure, respectively, compared to untreated controls (Figure 12M–O).

Western blot analysis of cell lysates obtained 24h after TNF-α stimulation of primary microglia showed a 7.1-fold increase in the short isoform of PDE4B, PDE4B2 (MW ~68kDa), but not PDE4A1 (Figure 13). Similarly, IL-1β also increased only PDE4B2 (3.3-fold) 24h after stimulation of primary microglia (Figure 13).

PDE4B mRNA and PDE4B2 protein was induced acutely following SCI during the period of injury-induced microglial cell activation and was expressed in the majority of OX-42$^+$ microglia-macrophages

We next examined the temporal profile of PDE4B expression and production following SCI as well as its cellular context, in $OX\text{-}42^+$ microglia-macrophages (Figure 14). Quantitative PCR for *pde4b* within the injury epicenter from 2h to 8wk following SCI showed a biphasic increase in expression, at 2–24h (peak at 2h, 2.2-fold increase; Figure 14A) and at 4–8wk post-injury (peak at 4wk, 2.0-fold increase). Western blot analysis showed a significant up-regulation of PDE4B2, with an apparent molecular weight of 68kDa, from 24h (2-fold) to 1wk post-SCI (1.5-fold), which peaked at 3d (2.4-fold) and had returned to uninjured control levels by 4wk (Figure 14B). To examine the protein production of PDE4 specifically within microglia we performed flow cytometric analysis of tissue from the injury epicenter at 3d post-SCI and gated $OX\text{-}42^+/PDE4A^-$, $OX\text{-}42^+/PDE4A^+$ and $OX\text{-}42^+/PDE4B^+$ cells. While only a modest percentage of $OX\text{-}42^+$ cells were immunoreactive for PDE4A (Average, 12.1%), the majority were $PDE4B^+$ (Average, 65.9%; Figure 14C).

PDE4B was localized to activated, but not inactive, microglia following acute SCI and TBI

To further confirm the identity of the cell type(s) expressing PDE4B after CNS injury we next examined the co-localization of PDE4B in $OX\text{-}42^+$ microglia-macrophages at 24h after SCI or TBI in tissue sections using immunohistochemistry. PDE4B was not expressed in either uninjured spinal cord or cortex (Supplemental Figure 1), nor was PDE4B found within resting, inactive microglia. At 24h following SCI, PDE4B was highly expressed within the lesion site and immediate injury penumbra, where $OX\text{-}42^+$ activated microglia were located (Figure 15A–D). Examination of PDE4B:OX-42 co-localization revealed that many $OX\text{-}42^+$ microglia expressed PDE4B, though there were $OX\text{-}42^+$ cells present further from the lesion that were not $PDE4B^+$ and some $PDE4^+$ cells found within the lesion that were not immunoreactive for OX-42. In injured brain at 24h after trauma, PDE4B immunostaining was found both within the gray matter of the injured cortex as well as in the white matter of the adjacent corpus callosum (Figure 15E–H). In both areas, PDE4B was always co-localized with $OX\text{-}42^+$ microglia. PDE4B immunoreactivity appeared to be predominantly nuclear. PDE4B appeared not to be localized to $OX\text{-}42^+$ microglia that exhibited a stellate appearance (inactive) or $OX\text{-}42^+$ foamy macrophages.

Discussion

Our studies demonstrate that not only are cyclic AMP levels critical for suppressing immune cell activation and pro-inflammatory cytokine production (Aronoff et al., 2004; Ghosh and Pearse, 2010), but that pro-inflammatory cytokines conversely regulate cyclic AMP signaling in microglia. This work sheds additional light on the intricacies of the intracellular signaling cascades involved in the auto-regulatory loop of pro-inflammatory cytokine-induced microglial cell activation (Aloisi, 2001; Pearse et al., 2004a). Specifically, in the present study we demonstrate that both TNF-α and IL-1β trigger a rapid and profound reduction in microglia (EOC2) cyclic AMP, which occurs as a biphasic change with IL-1β but was a persistent suppression with TNF-α through 24h. The effect of these cytokines in down-regulating cyclic AMP was also confirmed in primary microglia. The involvement of PDE4 in cyclic AMP reductions within microglia in response to both TNF-α and IL-1β was identified by the simultaneous addition of the PDE4 inhibitor Rolipram, which abrogated these effects. We show that PDE4A1 and PDEB2 were up-regulated in both EOC2 and primary microglia by these pro-inflammatory cytokines. The use of molecular knockdown with interference RNA demonstrated that PDE4B2 was involved in the down-regulation of cyclic AMP in activated microglia following TNF-α stimulation; future studies seek to identify whether PDE4A1 shares a similar function. In models of CNS injury, SCI and TBI, injury-induced PDE4B2 was demonstrated during the peak of microglia activation (Pineau and Lacroix, 2007); flow cytometry and immunohistochemistry showed that PDE4B expression was largely restricted to OX-42^{+} activated microglia and macrophages. Importantly, the current study demonstrates the putative therapeutic potential of targeting PDE4B2 to reverse microglial cell activation after CNS injury and neurodegenerative diseases where microglia activation is implicated as a primary cause of tissue injury and neurological dysfunction (Kreutzberg, 1996).

TNF-α and IL-1β are among the most important and pleiotropic cytokines in regulating inflammatory and immune responses in the CNS following trauma, infections and in chronic neurodegenerative or demyelinating disorders (Bartholdi and Schwab, 1997; Wang et al., 1996). TNF-α and IL-1β interact with their receptors TNFR1/2 or IL1R1/2, respectively, which are found on microglia (Dopp et al., 1997; Wang et al., 2006), mediating the gene expression of a number of cytokines and chemokines through the ERK, p38, JNK and NFκB intracellular signaling pathways that further potentiate immune cell activation, migration, phagocytosis and antigen presentation (Weber et al., 2010). A key component of the activation of a number of immune cell types (neutrophils, macrophages, microglia and T cells), is the down-regulation of cyclic AMP, which appears to maintain immune cell inactivation through the persistent suppression of pro-inflammatory cytokine and chemokine gene expression (Minguet et al., 2005). Exposure of immune cells to a variety of activating stimuli from endotoxins to phospholipids and cytokines produces a rapid reduction in cyclic AMP and the initiation of morphological and immunophenotypical changes that are characteristic of cellular reactivity. In the current study we show that stimulation of naïve EOC2 microglia with either TNF-α or IL-1β, to induce their activation, produces a rapid (within 30min) and dramatic (>90%) reduction in cyclic AMP. Simultaneous addition of the PDE4 inhibitor Rolipram, to prevent cyclic AMP hydrolysis, significantly abrogated cyclic

AMP reductions implying that PDE4 activity was essential to pro-inflammatory cytokine-induced cyclic AMP decreases. The observed down-regulation in cyclic AMP levels was confirmed in primary microglia, supporting the physiological relevance of the EOC2 microglial cell line used to examine this effect.

Temporal examination of cyclic AMP changes in response to cytokine stimulation revealed significant differences in microglial cyclic AMP levels following TNF-α and IL-1β. The observed disparity between cytokines, with a transient and complete cyclic AMP recovery at 1h following IL-1β compared to a persistent decrease through 24h with TNF-α, may be due to differences in the inflammatory gene expression programs they induce (Ortis et al., 2010). One such example is IL-1β's strong induction of cyclooxygenase-2 (COX-2) expression and prostanoid production, which can then in turn act to elevate cyclic AMP; TNF-α induces only weak COX-2 expression (Levi et al., 1998). IL-1β can also increase the expression of the cyclic AMP elevating peptide, pituitary-adenylate-cyclase-activating polypeptide (PACAP; Hannibal et al., 1999). It is also possible that this rebound in cyclic AMP levels at 1h after IL-1β stimulation could be responsible for triggering the observed later increase in PDE activity and reductions in cyclic AMP levels through 24 h. While TNF-α and IL-1β appear to produce similar phenotypical changes in microglia, it is not yet clear whether differences in the way these cytokines affect cyclic AMP-PDE signaling could provide functionally distinct cellular responses.

Previous work by Patrizio (2004), using a very high concentration (50ng/mL) of TNF-α in a pre-treatment (4–24h) approach, rather than simultaneous addition in activated microglia exposed to a combination of forskolin (FSK) and the PDE inhibitor 3-isobutyl-1-methyl-xanthine (IBMX) to promote cyclic AMP accumulation, showed that TNF-α in this paradigm could reverse cyclic AMP accumulation independent of PDE. The inhibition of cyclic AMP accumulation appeared to be due to a down-regulation of adenylyl cyclase activity through an NFκB-regulated mechanism. The previous work differs significantly from the current study in which we have examined the transition of naïve microglia to a morphologically and immunophenotypically active cell by TNF-α (or IL-1β) where homeostatic cyclic AMP levels are proposed to be responsible for maintaining microglia in an inactive state (Bourne et al., 1974; Steininger et al., 2011). While we demonstrate in the acute post-cytokine stimulation period (within 3 h) that PDE4 inhibition can reverse the inhibitory effects of TNF-α and IL-1β on cyclic AMP, implying that initial changes are due to cyclic AMP hydrolysis, persistent cyclic AMP reductions could also involve a down-regulation of adenylyl cyclase activity as suggested by Patrizio (2004) once the paradigm switches from an initial transition to the maintenance of microglia activation. Similar to the negative regulation of adenylyl cyclase activity by TNF-α through NFκB, it is also likely that TNF-α can also increase PDE4 expression and activity through NFκB. Although not examined in mononuclear phagocytes, TNF-α has been previously shown in carcinoma cells to increase PDE mRNA expression in a temporally-related fashion to NFκB activation (Pang et al., 1992). Converse to cytokine-induced reductions in cyclic AMP signaling, cyclic AMP can antagonize immune cell activation and function through the suppression of promoter activity of pro-activation genes by DNA bound, phosphorylated CREB (Wen et al., 2010), the inhibition of NFκB signaling by phosphorylated PKA (Neumann et al., 1995), or through the actions of EPAC (Steininger et al., 2011).

Studies using other immune cell activators, lipopolysaccharide (LPS) or interferon-γ (IFN-γ), in activated microglia cultures have shown that pre-treatment for 24h, but not post-treatment or simultaneous addition, can retard cyclic AMP accumulation in response to the β-adrenergic agonist, isoproterenol, adenylyl cyclase activator FSK or prostaglandin E_2 (PGE_2) (Patrizio et al., 1995). Like the current study, PDE4 inhibition using Rolipram prevented the inhibitory effects of LPS and IFN-γ on induced cyclic AMP accumulation.

Examination of *pde4* mRNA and protein changes in response to TNF-α and IL-1β revealed, like their cyclic AMP effects, that significant differences existed among the pro-inflammatory cytokines in *pde4* regulation. While both TNF-α and IL-1β increased *pde4b* expression, only IL-1β additionally increased *pde4a* and *pde4d*. Work to date examining *pde4* gene promoter regulatory elements for *pde4a* (McCahill et al., 2008), *pde4b* (D'Sa et al., 2002), and *pde4d* (D'Sa et al., 2002; Le Jeune et al., 2002) have identified cyclic AMP responsive elements (CRE) that allow *pde4* expression to be regulated, in most cases positively, by cyclic AMP-CREB as a feedback mechanism for reducing cyclic AMP levels. Indeed, the observed differences in *pde4* mRNA expression between the cytokines may be related to the observed transient recovery of cyclic AMP after IL-1β that could lead to the additional induction of *pde4a* and *d* expression.

Immunoblotting demonstrated that TNF-α stimulation induced an increase in PDE4A1 and PDE4B2 while PDE4B2 was also increased with IL-1β in microglia. PDE4B2 is the short-form isozyme (~68 kDa) of PDE4B that contains an upstream conserved region-2 (UCR-2) but not UCR-1, meaning that its activity is not regulated by PKA phosphorylation, though ERK phosphorylation enhances its activity (Baillie et al., 2000). Expression of the PDE4B gene has been shown to be induced in many immune cell populations (Baillie et al., 2000; MacKenzie and Houslay, 2000; Sebastiani et al., 2006), including circulating human monocytes (Wang et al., 1999) in response to immune activators, like LPS. The importance of PDE4B in regulating inflammatory responses was demonstrated by Jin et al. (2002; 2005) in which LPS-induced TNF-α production was significantly attenuated in peripheral leukocytes and macrophages from PDE4B, but not PDE4D, knockout mice. PDE4B2 has been shown to be the only PDE4B variant with increased expression around blood vessels and parenchyma in infiltrating T cells and macrophages/microglia following the induction of experimental autoimmune encephalomyelitis (EAE; Reyes-Irisarri et al., 2007). PDE4B2 has also been demonstrated to enhance T cell activation and IL-2 production following compartmentalization in lipid rafts close to the immunologic synapse and sites of high cyclic AMP generation early in the T cell activation process (Arp et al., 2003). It therefore appears that PDE4B2 is a key regulator of immune cell activation.

Although both TNF-α and IL-1β increased PDE4B, immunocytochemistry revealed a very distinct difference in the subcellular localization of PDE4B following exposure to these pro-inflammatory cytokines at 3, but not 24 hours. While PDE4B was present within the cytoplasm at 3 hours following IL-1β, after TNF-α, PDE4B was predominantly localized to the nucleus of microglia. It has shown that both PDE4B (Huston et al., 2008; Lugnier et al., 1999) and PDE4D (Chandrasekaran et al., 2008; Lugnier et al., 1999) can be present within the nucleus of other cell types including human embryonic kidney cells (HEK-B2), mouse NIH-3T3 fibroblasts and cardiac cells. Previous studies had suggested a role for cyclic

AMP-dependent PDEs within the nucleus through putative identification of cyclic AMP-specific PDE activity (Londesborough and Jönkkäri, 1982), high cyclic AMP hydrolytic activity in the nucleus (Lugnier et al., 1999) and PDE binding to chromatin (Lupidi et al., 1990). Huston and colleagues (2008) demonstrated that the ability of EPAC to trigger nuclear/cytoplasmic trafficking of DNA-dependent protein kinase (DNA-PK), a critical kinase that acts to repair double-stranded breaks (DSBs) in damaged DNA and that also phosphorylates the cell survival kinase PKB/Akt in the cytoplasm, is primarily gated by the level of cyclic AMP degradation through the cyclic AMP-hydrolyzing activity of nuclear PDE4B. In this paradigm PDE4B was constitutively localized to the nucleus. Although cytokine stimulation of microglia often leads to their apoptosis (Jones et al., 1997), it is yet to be determined what is the role of the transient nuclear translocation of PDE4B from the cytoplasm in activated microglia in the current study and whether such translocation involves either a cyclic AMP hydrolytic function of PDE4B in the nucleus or whether PDE4B participates as a scaffolding molecule with other signaling intermediaries. Through the use of PredictNLS we have shown that PDE4B2 may contain a putative [DE]RxKKKK NLS sequence, which was highly conserved among species.

Due to the importance of PDE4B in regulating cellular activation and immune responses in other immune cell types as well as its persistent up-regulation in microglia following stimulation with either TNF-α or IL-1β, as observed in the current study, we next employed an interference RNA approach to determine its role in microglial cyclic AMP changes in response to TNF-α. We demonstrated that this approach produces substantial reductions in PDE4B and prevented TNF-α-induced decreases in cyclic AMP. Therefore, like other immune cells, macrophages and leukocytes (Jin et al., 2002; 2005; Wang et al., 1999), PDE4B appears to be the major PDE4 enzyme responsible for cyclic AMP hydrolysis and ensuing cell activation in microglia in response to pro-inflammatory cytokines.

To determine the significance of these *in vitro* changes to CNS injury, we next examined temporal changes and cellular localization of PDE4B in two models of CNS trauma, SCI and TBI. Following SCI there was a rapid increase in both PDE4B2 mRNA (2h) and protein (24h) that persisted during the peak of microglia activation. Flow cytometry of OX-42^{+} microglia-macrophages confirmed that among PDE4 gene products, PDE4B was the protein that was most highly expressed in these cells acutely post-injury. Immunohistochemistry confirmed that PDE4B was localized to activated OX-42^{+} microglia both within and near to the injury site after both SCI, in agreement with Whitaker et al. (2008), and TBI, though it was not present within detectable amounts in uninjured tissue from the same CNS regions or within OX-42 microglia that appeared to have an inactive or less activated phenotype (lacking the morphology of a fully-activated phagocyte).

Here we demonstrate that the pro-inflammatory cytokines, TNF-α and IL1-β potently reduce cyclic AMP within microglia as they transition to a morphologically and immunophenotypically activated phenotype. These changes appear to be related to an increase in cyclic AMP-specific PDE activity that is largely mediated through PDE4B2. Interestingly, PDE4B2 may act both within the cytoplasm and nucleus to achieve these changes and initiate a gene expression program that results in microglial cell activation. Importantly we demonstrate that such changes in PDE4B also occur in microglia-

macrophages following CNS injury, after both SCI and TBI, like EAE (Reyes-Irisarri et al., 2007), suggesting that selective targeting of PDE4B2 may be a promising therapeutic direction for restricting microglial cell activation and providing neuroprotection after CNS injury, a result that has been shown previously with the broad spectrum PDE4 inhibitor, Rolipram.

Supplementary Material

Refer to Web version on PubMed Central for supplementary material.

Acknowledgments

We would like to thank Dr. Alexander Marcillo and Paulo Diaz from The Miami Project Animal Core Facility for inducing contusion injuries as well as Denise Koivisto and Ramon German for performing animal care. We would like to gratefully acknowledge Ofelia Furones-Alonso for performing traumatic brain injury and Coleen Atkins for providing tissue samples. Amit Patel is thanked for assistance with immunohistochemistry and Dr. Beata Frydel for image analysis. Wai-Man Chan and Jeffrey Datto are acknowledged for their help in proof-reading of the manuscript.

Funding: This work was supported by: NIH NINDS Grants 056072 (W.D.D.) and 056281 (D.D.P.) and the Miami Project to Cure Paralysis.

References

Aloisi F. Immune function of microglia. Glia. 2001; 36:165–79. [PubMed: 11596125]

Aronoff DM, Canetti C, Peters-Golden M. Prostaglandin E2 inhibits alveolar macrophage phagocytosis through an E-prostanoid 2 receptor-mediated increase in intracellular cyclic AMP. J Immunol. 2004; 173:559–65. [PubMed: 15210817]

Arp J, Kirchhof MG, Baroja ML, Nazarian SH, Chau TA, Strathdee CA, Ball EH, Madrenas J. Regulation of T-cell activation by phosphodiesterase 4B2 requires its dynamic redistribution during immunological synapse formation. Mol Cell Biol. 2003; 23:8042–57. [PubMed: 14585965]

Atkins CM, Oliva AA Jr, Alonso OF, Pearse DD, Bramlett HM, Dietrich WD. Modulation of the cAMP signaling pathway after traumatic brain injury. Exp Neurol. 2007; 208:145–58. [PubMed: 17916353]

Baillie GS, MacKenzie SJ, McPhee I, Houslay MD. Sub-family selective actions in the ability of Erk2 MAP kinase to phosphorylate and regulate the activity of PDE4 cyclic AMP-specific phosphodiesterases. Br J Pharmacol. 2000; 131:811–19. [PubMed: 11030732]

Bao F, Fleming JC, Golshani R, Pearse DD, Kasabov L, Brown A, Weaver LC. A selective phosphodiesterase-4 inhibitor reduces leukocyte infiltration, oxidative processes, and tissue damage after spinal cord injury. J Neurotrauma. 2011; 28:1035–49. [PubMed: 21355819]

Barakat DJ, Gaglani SM, Neravetla SR, Sanchez AR, Andrade CM, Pressman Y, Puzis R, Garg MS, Bunge MB, Pearse DD. Survival, integration, and axon growth support of glia transplanted into the chronically contused spinal cord. Cell Transplant. 2005; 14:225–40. [PubMed: 15929557]

Bartholdi D, Schwab ME. Expression of pro-inflammatory cytokine and chemokine mRNA upon experimental spinal cord injury in mouse: an in situ hybridization study. Eur J Neurosci. 1997; 9:1422–1438. [PubMed: 9240400]

Baud V, Karin M. Signal transduction by tumor necrosis factor and its relatives. Trends Cell Biol. 2001; 11:372–7. [PubMed: 11514191]

Bethea JR, Nagashima H, Acosta MC, Briceno C, Gomez F, Marcillo AE, Loor K, Green J, Dietrich WD. Systemically administered interleukin-10 reduces tumor necrosis factor-alpha production and significantly improves functional recovery following traumatic spinal cord injury in rats. J Neurotrauma. 1999; 16:851–863. [PubMed: 10547095]

Bourne HR, Lichtenstein LM, Melmon KL, Henney CS, Weinstein Y, Shearer GM. Modulation of inflammation and immunity by cyclic AMP. Science. 1974; 5:19–28. [PubMed: 4131281]

Breder CD, Tsujimoto M, Terano Y, Scott DW, Saper CB. Distribution and characterization of tumor necrosis factor-alpha-like immunoreactivity in the murine central nervous system. J Comp Neurol. 1993; 337:543–67. [PubMed: 8288770]

Caggiano AO, Kraig RP. Prostaglandin E receptor subtypes in cultured rat microglia and their role in reducing lipopolysaccharide-induced interleukin-1beta production. J Neurochem. 1999; 72:565–75. [PubMed: 9930728]

Chandrasekaran A, Toh KY, Low SH, Tay SK, Brenner S, Goh DL. Identification and characterization of novel mouse PDE4D isoforms: molecular cloning, subcellular distribution and detection of isoform-specific intracellular localization signals. Cell Signal. 2008; 20:139–53. [PubMed: 18006274]

Damoiseaux JG, Döpp EA, Calame W, Chao D, MacPherson GG, Dijkstra CD. Rat macrophage lysosomal membrane antigen recognized by monoclonal antibody ED1. Immunology. 1994; 83:140–147. [PubMed: 7821959]

Dopp JM, Mackenzie-Graham A, Otero GC, Merrill JE. Differential expression, cytokine modulation, and specific functions of type-1 and type-2 tumor. necrosis factor receptors in rat glia. J Neuroimmunol. 1997; 75:104–112. [PubMed: 9143243]

D'Sa C, Tolbert LM, Conti M, Duman RS. Regulation of cAMP-specific phosphodiesterases type 4B and 4D (PDE4) splice variants by cAMP signaling in primary cortical neurons. J Neurochem. 2002; 81:745–57. [PubMed: 12065634]

Dunne A, O'Neill LA. The interleukin-1 receptor/Toll-like receptor superfamily: signal transduction during inflammation and host defense. Sci STKE. 2003; 25:171.

Ghosh M, Tuesta LM, Puentes R, Patel S, Melendez K, El Maarouf A, Rutishauser U, Pearse DD. Extensive cell migration, axon regeneration, and improved function with polysialic acid-modified Schwann cells after spinal cord injury. Glia. 2012; 60:979–992. [PubMed: 22460918]

Ghosh P, Pearse DD. Cyclic AMP-specific PDEs: A promising therapeutic target for CNS repair. Transl Neurosci. 2010; 1:101–105.

Goodman JC, Van M, Gopinath SP, Robertson CS. Pro-inflammatory and pro-apoptotic elements of the neuroinflammatory response are activated in traumatic brain injury. Acta Neurochir Suppl. 2008; 102:437–9. [PubMed: 19388362]

Gruner JA. A monitored contusion model of spinal cord injury in the rat. J Neurotrauma. 1992; 9:123–6. [PubMed: 1404425]

Hannibal J, Jessop DS, Fahrenkrug J, Harbuz MS, Larsen PJ. PACAP gene expression in neurons of the rat hypothalamo-pituitary-adrenocortical axis is induced by endotoxin and interleukin-1beta. Neuroendocrinology. 1999; 70:73–82. [PubMed: 10420095]

Hurley SD, Walter SA, Semple-Rowland SL, Streit WJ. Cytokine transcripts expressed by microglia in vitro are not expressed by ameboid microglia of the developing rat central nervous system. Glia. 1999; 25:304–309. [PubMed: 9932876]

Huston E, Lynch MJ, Mohamed A, Collins DM, Hill EV, MacLeod R, Krause E, Baillie GS, Houslay MD. EPAC and PKA allow cAMP dual control over DNA-PK nuclear translocation. Proc Natl Acad Sci U S A. 2008; 105:12791–6. [PubMed: 18728186]

Jin SL, Conti M. Induction of the cyclic nucleotide phosphodiesterase PDE4B is essential for LPS-activated TNF-alpha responses. Proc Natl Acad Sci U S A. 2002; 28:7628–33. [PubMed: 12032334]

Jin SL, Lan L, Zoudilova M, Conti M. Specific role of phosphodiesterase 4B in lipopolysaccharide-induced signaling in mouse macrophages. J Immunol. 2005; 175:1523–31. [PubMed: 16034090]

Jones LL, Banati RB, Graeber MB, Bonfanti L, Raivich G, Kreutzberg GW. Population control of microglia: does apoptosis play a role? J Neurocytol. 1997; 26:755–70. [PubMed: 9426172]

Kinoshita K, Chatzipanteli K, Vitarbo E, Truettner JS, Alonso OF, Dietrich WD. Interleukin-1beta messenger ribonucleic acid and protein levels after fluid-percussion brain injury in rats: importance of injury severity and brain temperature. Neurosurgery. 2002; 51:195–203. [PubMed: 12182417]

Kita T, Liu L, Tanaka N, Kinoshita Y. The expression of tumor necrosis factor-alpha in the rat brain after fluid percussive injury. Int J Legal Med. 1997; 110:305–11. [PubMed: 9387012]

Kleppisch T. Phosphodiesterases in the central nervous system. Handb Exp Pharmacol. 2009; 191:71–92. [PubMed: 19089326]

Kreutzberg GW. Microglia: A sensor for pathological events in the CNS. Trends Neurosci. 1996; 19:312–8. [PubMed: 8843599]

Le Jeune IR, Shepherd M, Van Heeke G, Houslay MD, Hall IP. Cyclic AMP-dependent transcriptional up-regulation of phosphodiesterase 4D5 in human airway smooth muscle cells. Identification and characterization of a novel PDE4D5 promoter. J Biol Chem. 2002; 277:35980–9. [PubMed: 12121997]

Levi G, Minghetti L, Aloisi F. Regulation of prostanoid synthesis in microglial cells and effects of prostaglandin E2 on microglial functions. Biochimie. 1998; 80:899–904. [PubMed: 9893949]

Londesborough J, Jönkkäri L. Low Km cyclic AMP phosphodiesterase of yeast may be bound to ribosomes associated with the nucleus. Mol Cell Biochem. 1982; 23:65–71. [PubMed: 6287208]

Lucin KM, Wyss-Coray T. Immune activation in brain aging and neurodegeneration: too much or too little? Neuron. 2009; 64:110–22. [PubMed: 19840553]

Lugnier C, Keravis T, Le Bec A, Pauvert O, Proteau S, Rousseau E. Characterization of cyclic nucleotide phosphodiesterase isoforms associated to isolated cardiac nuclei. Biochim Biophys Acta. 1999; 16:431–46. [PubMed: 10564757]

Lupidi G, Eufemi M, Luciani S, Ferraro A, Riva F. 3′-5′ cAMP phosphodiesterase in pig liver nuclei. Ital J Biochem. 1990; 39:30–7. [PubMed: 2157681]

Ma D, Wu P, Egan RW, Billah MM, Wang P. Phosphodiesterase 4B gene transcription is activated by lipopolysaccharide and inhibited by interleukin-10 in human monocytes. Mol Pharmacol. 1999; 55:50–7. [PubMed: 9882697]

MacKenzie SJ, Houslay MD. Action of rolipram on specific PDE4 cAMP phosphodiesterase isoforms and on the phosphorylation of cAMP-response-element-binding protein (CREB) and p38 mitogen-activated protein (MAP) kinase in U937 monocytic cells. Biochem J. 2000; 347:571–8. [PubMed: 10749688]

McCahill A, Campbell L, McSorley T, Sood A, Lynch MJ, Li X, Yan C, Baillie GS, Houslay MD. In cardiac myocytes, cAMP elevation triggers the down-regulation of transcripts and promoter activity for cyclic AMP phosphodiesterase-4A10 (PDE4A10). Cell Signal. 2008; 11:2071–83. [PubMed: 18721873]

Mecha M, Iñigo PM, Mestre L, Hernangómez M, Borrell J, Guaza C. An easy and fast way to obtain a high number of glial cells from rat cerebral tissue: A beginners approach. Protocol Exchange. 2011; 3(10):2011.

Minguet S, Huber M, Rosenkranz L, Schamel WW, Reth M, Brummer T. Adenosine and cAMP are potent inhibitors of the NF-kappa B pathway downstream of immunoreceptors. Eur J Immunol. 2005; 35:31–41. [PubMed: 15580656]

Neumann M, Grieshammer T, Chuvpilo S, Kneitz B, Lohoff M, Schimpl A, Franza BR Jr, Serfling E. RelA/p65 is a molecular target for the immunosuppressive action of protein kinase A. EMBO J. 1995; 14:1991–2004. [PubMed: 7744006]

Ortis F, Naamane N, Flamez D, Ladrière L, Moore F, Cunha DA, Colli ML, Thykjaer T, Thorsen K, Orntoft TF, Eizirik DL. Cytokines interleukin-1beta and tumor necrosis factor-alpha regulate different transcriptional and alternative splicing networks in primary beta-cells. Diabetes. 2010; 59:358–74. [PubMed: 19934004]

Pang XP, Ross NS, Park M, Juillard GJ, Stanley TM, Hershman JM. Tumor necrosis factor-alpha activates nuclear factor kappa B and induces manganous superoxide dismutase and phosphodiesterase mRNA in human papillary thyroid carcinoma cells. J Biol Chem. 1992; 267:12826–30. [PubMed: 1320006]

Patel V, Joseph G, Patel A, Patel S, Bustin D, Mawson D, Tuesta LM, Puentes R, Ghosh M, Pearse DD. Suspension matrices for improved Schwann-cell survival after implantation into the injured rat spinal cord. J Neurotrauma. 2010; 27:789–801. [PubMed: 20144012]

Patrizio M, Costa T, Levi G. Interferon-gamma and lipopolysaccharide reduce cAMP responses in cultured glial cells: reversal by a type IV phosphodiesterase inhibitor. Glia. 1995; 14:94–100. [PubMed: 7558245]

Patrizio M. Tumor necrosis factor reduces cAMP production in rat microglia. Glia. 2004; 48:241–9. [PubMed: 15390118]

Pearse DD, Bushell G, Leah JD. Fos and Krox in the thalamus after C-fiber stimulation: coincident-input-dependent expression, expression across somatotopic boundaries, and nucleolar translocation. Neuroscience. 2001 Jun.107:143–59. [PubMed: 11744254]

Pearse DD, Pereira FC, Stolyarova A, Barakat DJ, Bunge MB. Inhibition of tumour necrosis factor-alpha by antisense targeting produces immunophenotypical and morphological changes in injury-activated microglia and macrophages. Eur J Neurosci. 2004a; 20:3387–96. [PubMed: 15610171]

Pearse DD, Pereira FC, Marcillo AE, Bates ML, Berrocal YA, Filbin MT, Bunge MB. cAMP and Schwann cells promote axonal growth and functional recovery after spinal cord injury. Nat Med. 2004b; 10:610–6. [PubMed: 15156204]

Pearse D, Jarnagin K. Abating progressive tissue injury and preserving function after CNS trauma: The role of inflammation modulatory therapies. Curr Opin Investig Drugs. 2010; 11:1207–10.

Pineau I, Lacroix S. Proinflammatory cytokine synthesis in the injured mouse spinal cord: multiphasic expression pattern and identification of the cell types involved. J Comp Neurol. 2007; 500:267–85. [PubMed: 17111361]

Reyes-Irisarri E, Sánchez AJ, García-Merino JA, Mengod G. Selective induction of cAMP phosphodiesterase PDE4B2 expression in experimental autoimmune encephalomyelitis. J Neuropathol Exp Neurol. 2007; 66:923–31. [PubMed: 17917586]

Rice T, Larsen J, Rivest S, Yong VW. Characterization of the early neuroinflammation after spinal cord injury in mice. J Neuropathol Exp Neurol. 2007; 66:184–95. [PubMed: 17356380]

Schaal SM, Kitay BM, Cho KS, Lo TP Jr, Barakat DJ, Marcillo AE, Sanchez AR, Andrade CM, Pearse DD. Schwann cell transplantation improves reticulospinal axon growth and forelimb strength after severe cervical spinal cord contusion. Cell Transplant. 2007; 16:207–228. [PubMed: 17503734]

Sebastiani G, Morissette C, Lagacé C, Boulé M, Ouellette MJ, McLaughlin RW, Lacombe D, Gervais F, Tremblay P. The cAMP-specific phosphodiesterase 4B mediates Abeta-induced microglial activation. Neurobiol Aging. 2006; 27:691–701. [PubMed: 15993984]

Selmaj K, Raine CS, Farooq M, Norton WT, Brosnan CF. Cytokine cytotoxicity against oligodendrocytes. Apoptosis induced by lymphotoxin. J Immunol. 1991; 147:1522–1529. [PubMed: 1908877]

Semmler J, Wachtel H, Endres S. The specific type IV phosphodiesterase inhibitor rolipram suppresses tumor necrosis factor-alpha production by human mononuclear cells. Int J Immunopharmacol. 1993; 15:409–13. [PubMed: 8505151]

Serezani CH, Ballinger MN, Aronoff DM, Peters-Golden M. Cyclic AMP: master regulator of innate immune cell function. Am J Respir Cell Mol Biol. 2008; 39:127–132. [PubMed: 18323530]

Sharif SF, Hariri RJ, Chang VA, Barie PS, Wang RS, Ghajar JB. Human astrocyte production of tumour necrosis factor-alpha, interleukin-1 beta, and interleukin-6 following exposure to lipopolysaccharide endotoxin. Neurol Res. 1993; 15:109–12. [PubMed: 8099204]

Steininger TS, Stutz H, Kerschbaum HH. Beta-adrenergic stimulation suppresses phagocytosis via Epac activation in murine microglial cells. Brain Res. 2011; 1407:1–12. [PubMed: 21763641]

Streit WJ, Semple-Rowland SL, Hurley SD, Miller RC, Popovich PG, Stokes BT. Cytokine mRNA profiles in contused spinal cord and axotomized facial nucleus suggest a beneficial role for inflammation and gliosis. Exp Neurol. 1998; 152:74–87. [PubMed: 9682014]

Vitarbo EA, Chatzipanteli K, Kinoshita K, Truettner JS, Alonso OF, Dietrich WD. Tumor necrosis factor alpha expression and protein levels after fluid percussion injury in rats: the effect of injury severity and brain temperature. Neurosurgery. 2004; 55:416–24. [PubMed: 15271250]

Wajant H, Pfizenmaier K, Scheurich P. Tumor necrosis factor signaling. Cell Death Differ. 2003; 10:45–65. [PubMed: 12655295]

Walker WS, Gatewood J, Olivas E, Askew D, Havenith CEG. Mouse microglial cell lines differing in constitutive and interferon-γ-inducible antigen-presenting activities for naïve and memory CD4+ and CD8+ T cell. J Neuroimmunol. 1995; 63:163–174. [PubMed: 8550814]

Wang CX, Nuttin B, Heremans H, Dom R, Gybels J. Production of tumor necrosis factor in spinal cord following traumatic injury in rats. J Neuroimmunol. 1996; 69:151–156. [PubMed: 8823387]

Wang P, Wu P, Ohleth KM, Egan RW, Billah MM. Phosphodiesterase 4B2 is the predominant phosphodiesterase species and undergoes differential regulation of gene expression in human monocytes and neutrophils. Mol Pharmacol. 1999; 56:170–4. [PubMed: 10385698]

Wang XF, Huang LD, Yu PP, Hu JG, Yin L, Wang L, Xu XM, Lu PH. Upregulation of type I interleukin-1 receptor after traumatic spinal cord injury in adult rats. Acta Neuropathol. 2006; 111:220–8. [PubMed: 16456668]

Weber A, Wasiliew P, Kracht M. Interleukin-1 (IL-1) pathway. Sci Signal. 2010; 3:105–110.

Wen AY, Sakamoto KM, Miller LS. The role of the transcription factor CREB in immune function. J Immunol. 2010; 185:6413–9. [PubMed: 21084670]

Whitaker CM, Beaumont E, Wells MJ, Magnuson DS, Hetman M, Onifer SM. Rolipram attenuates acute oligodendrocyte death in the adult rat ventrolateral funiculus following contusive cervical spinal cord injury. Neurosci Lett. 2008; 438:200–4. [PubMed: 18455876]

Yakovlev AG, Faden AI. Sequential expression of c-fos proto-oncogene, TNF-alpha, and dynorphin genes in spinal cord following experimental traumatic injury. Mol Chem Neuropathol. 1994; 23:179–90. [PubMed: 7702707]

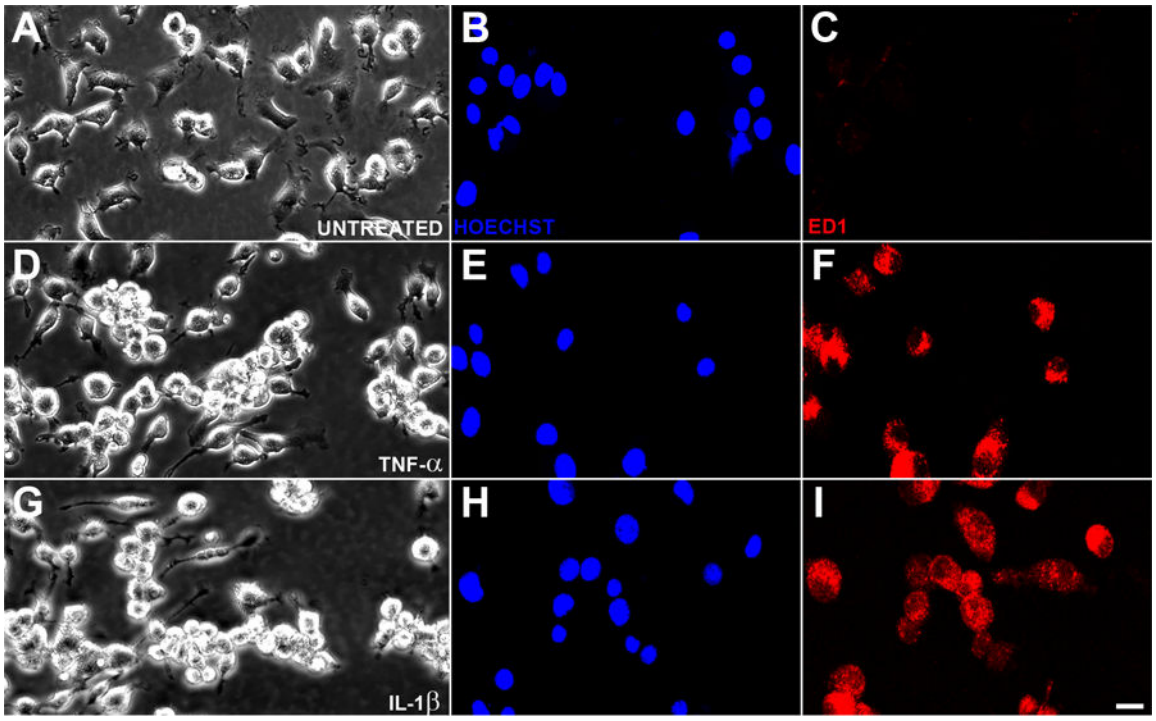

Figure 1. Stimulation of EOC2 microglia with TNF-α and IL-1β induced morphological and immunophenotypical changes characteristic of cell activation

A–C. Naïve microglia exhibited a stellate morphology with complex filopodial architecture under phase microscopy (**A**). The lysosomal protein macrosialin (ED1) was not expressed (**B–C**). **D–F.** Following stimulation with 10ng TNF-α for 24h, microglia underwent a pronounced morphological change to a rounded phenotype (**D**) and expressed ED1 (**E–F**). **G–I.** An indistinguishable morphological (**G**) and immunophenotypical change (**H–I**) occurred 24h after 5ng IL-1β challenge. All cultures were stained with Hoechst to identify cell nuclei. Scale bar = 15μm.

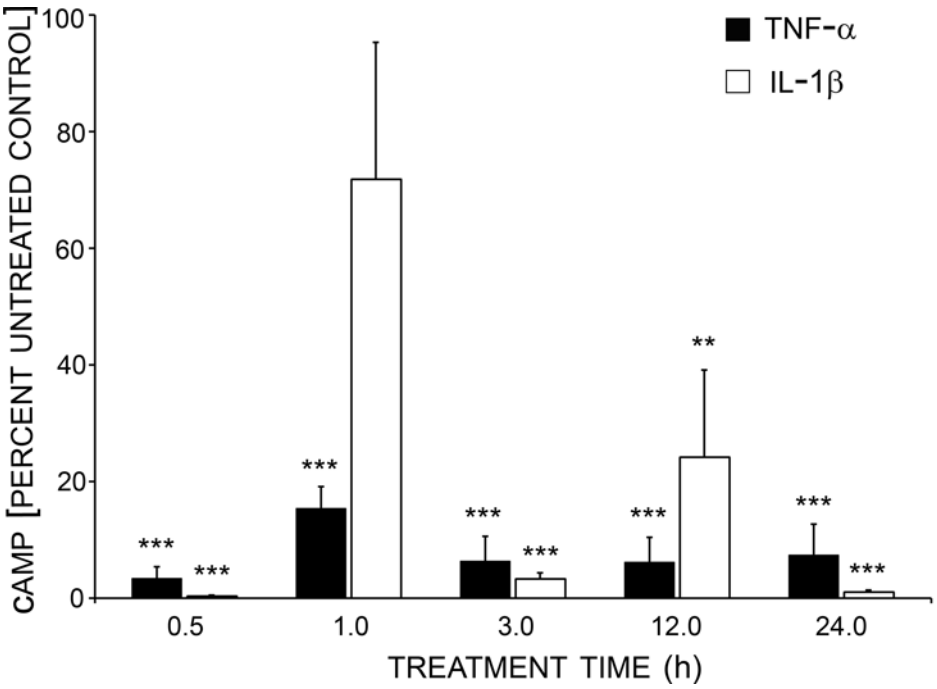

Figure 2. Pronounced and persistent reductions in EOC2 microglial cyclic AMP occurred following exposure to pro-inflammatory cytokines

Within 30min of TNF-α or IL-1β exposure a pronounced reduction in cyclic AMP was observed in microglia. In TNF-α-treated microglia, cyclic AMP levels remained persistently at this very low level through 24h while following IL-1β addition to microglia there were transient recoveries of cyclic AMP levels at 1 and 12h. Cyclic AMP levels are expressed as a percent of naïve controls. Results shown are the averages from 4 independent culture plate replicates for each treatment and time point examined. Errors are given as SEMs. Statistical significance to naïve controls; **p<0.01 and ***p<0.001.

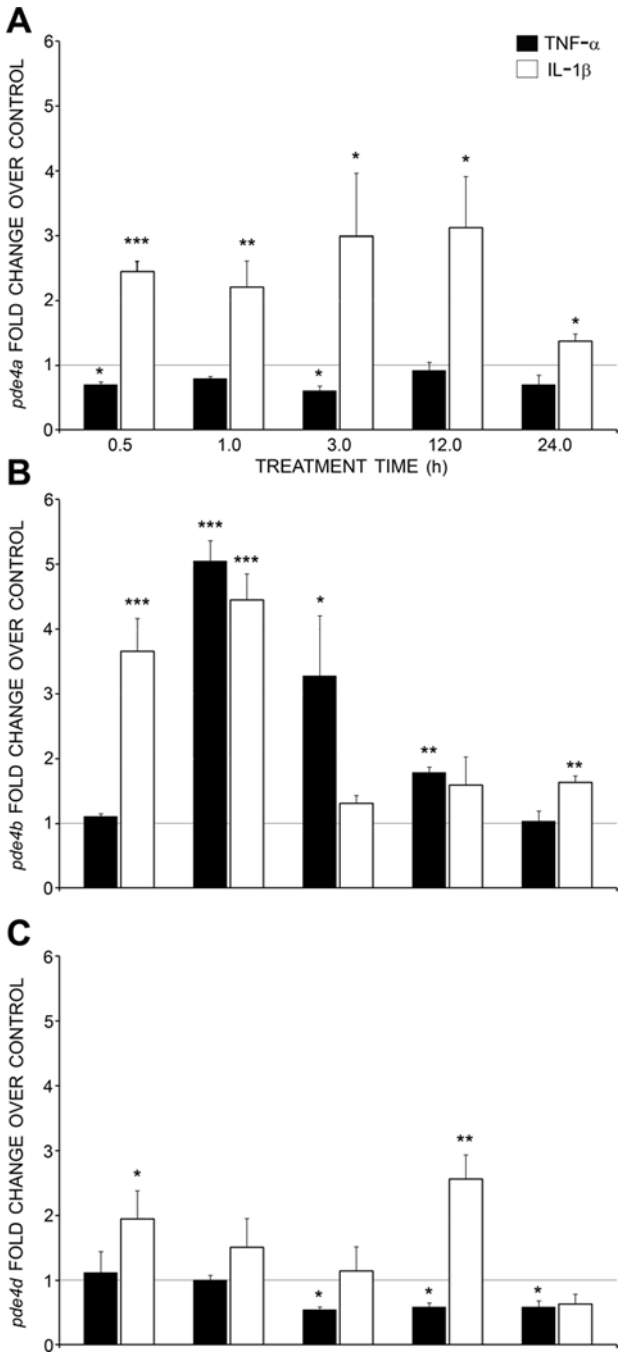

Figure 3. Both TNF-α and IL-1β increased expression of *pde4b* transcripts in EOC2 microglia while IL-1β also increased *pde4a* and *pde4d* expression

A. Following TNF-α-treatment of microglia there was a modest reduction in *pde4a* expression, however, IL-1β enhanced *pde4a* expression at all time points examined. **B.** A dramatic increase in *pde4b* expression following TNF-α exposure was observed beginning at 1h, with expression remaining significantly elevated through 12h. Stimulation of microglia with IL-1β produced a more rapid and transient increase in *pde4b* mRNA expression. **C.** For *pde4d* expression there was only a transient increase in expression at 12h

after IL-1β stimulation. The expression of *pde4* transcripts is expressed as a -fold change over their individual expression in naïve microglia. Results shown are the averages from 3 independent culture plate replicates for each treatment and time point examined. Errors are given as SEMs. Statistical significance to naïve controls; *p<0.05, **p<0.01 and ***p<0.001.

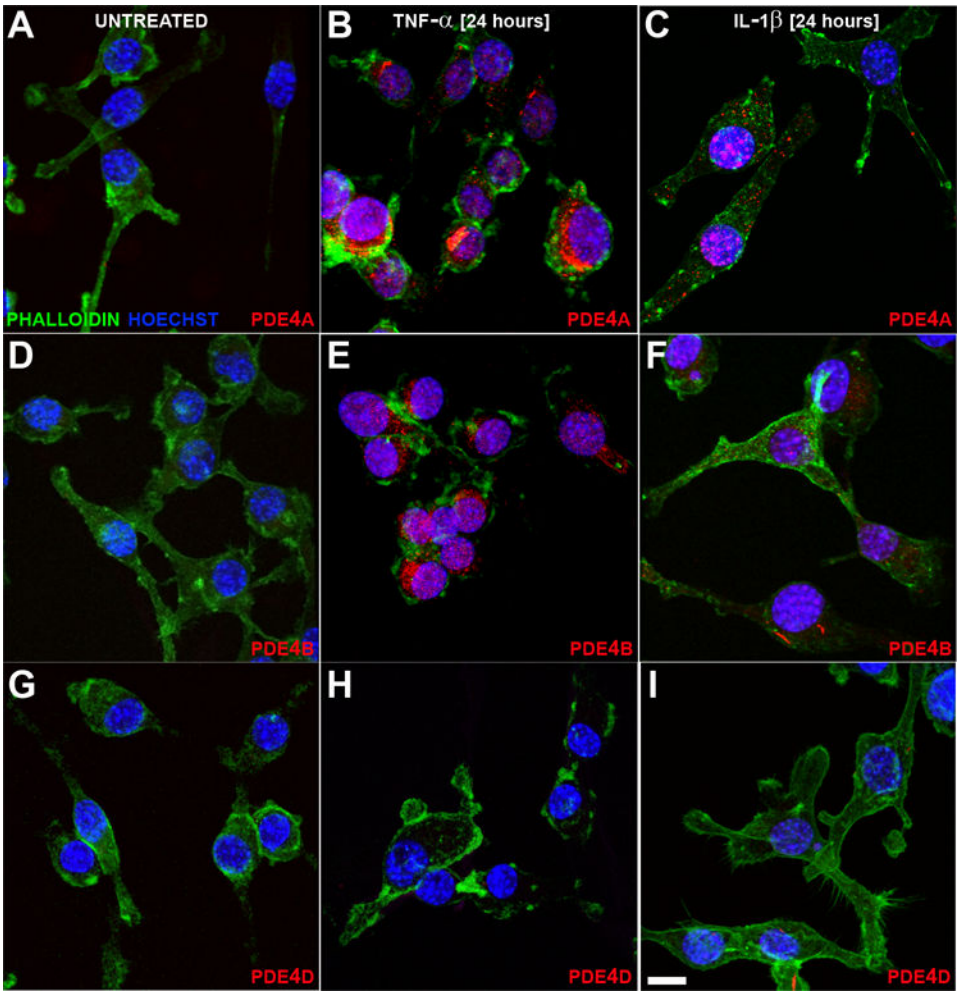

Figure 4. PDE4A and B, but not D, protein was observed in TNF-α and IL-1β stimulated EOC2 microglia by immunocytochemistry

A–C. In comparison to naïve microglia (**A**), where little PDE4A was detected, stimulation with TNF-α (**B**), and to a lesser degree IL-1β (**C**), significantly increased cytoplasmic and membrane PDE4A immunoreactivity in microglial cells at 24h. **D–F.** Similar to PDE4A, PDE4B immunoreactivity was low in naïve microglia (**D**). At 24h after TNF-α stimulation (**E**), but not IL-1β (**F**), increased cytoplasmic staining for PDE4B was evident. **G–I.** PDE4D immunoreactivity was not detectable in naïve (**G**) or TNF-α (**H**) and IL-1β (**I**) stimulated microglia. All cultures were stained with Phalloidin-Alexa 488 for cell morphology and Hoechst to identify nuclei. Scale bar = 10μm.

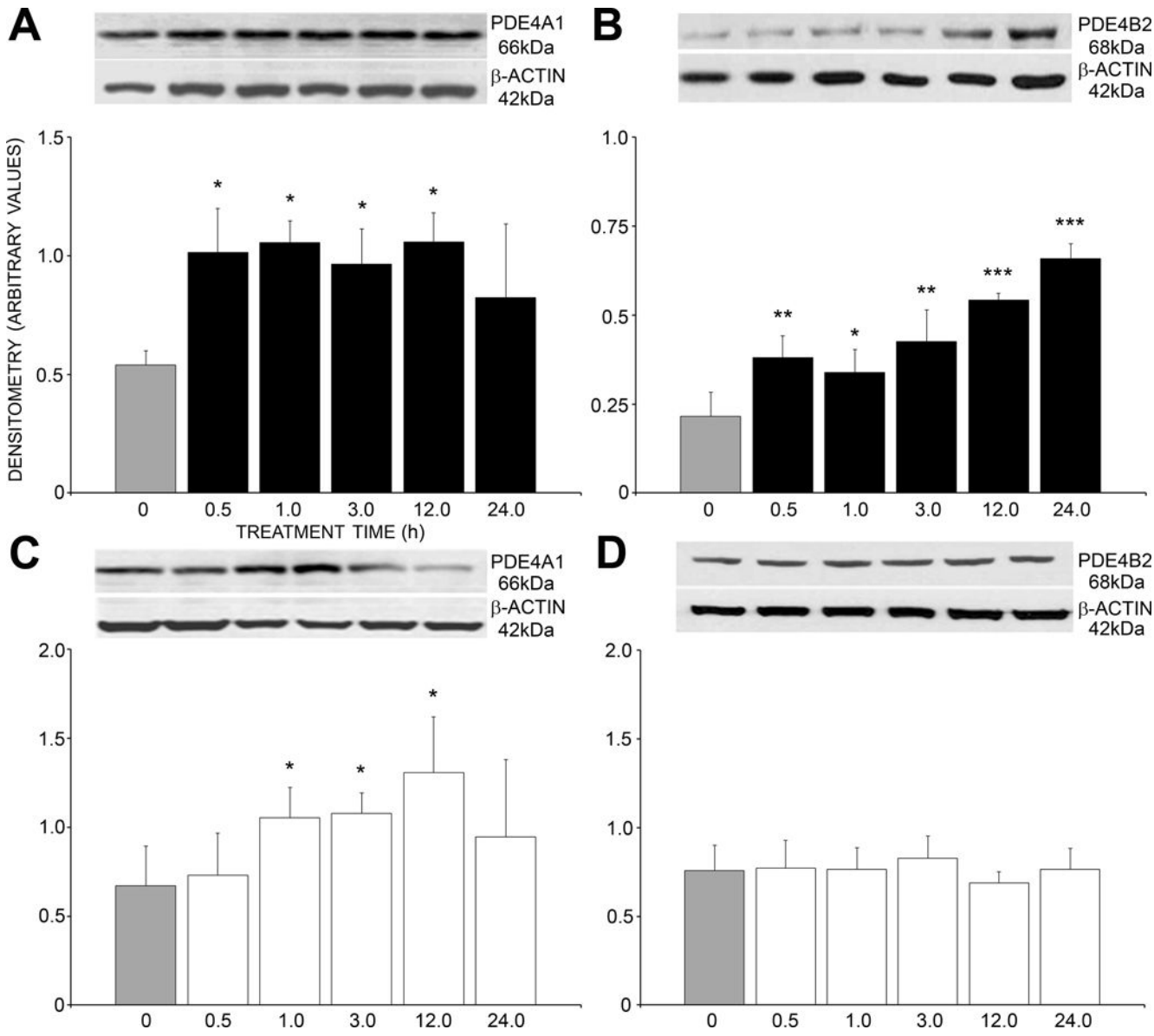

Figure 5. The exposure of EOC2 microglia to TNF-α increased the level of PDE4A1 and B2, while IL-1β enhanced only PDE4A1

A–B. TNF-α significantly increased both PDE4A1 (**A**; 66kDa; 30min to 12h) and PDE4B2 (**B**; 68kDa; 30min to 24h) protein in microglia compared to naïve controls (gray bars). **C–D.** An increase in PDE4A1 (**C**; 1 to 12h), but no change in PDE4B2 (**D**), was observed after IL-1β. No other molecular weight bands for either PDE4A or 4B were detected under the experimental conditions used and with the antibodies employed. PDE4D could not be detected by western blot in naïve or treated EOC2 microglia. Results shown are the averages from 5 independent culture plate replicates for each treatment and time point examined. Errors are given as SEMs. Statistical significance to naïve controls is indicated at *p<0.05, **p<0.01 and ***p<0.001.

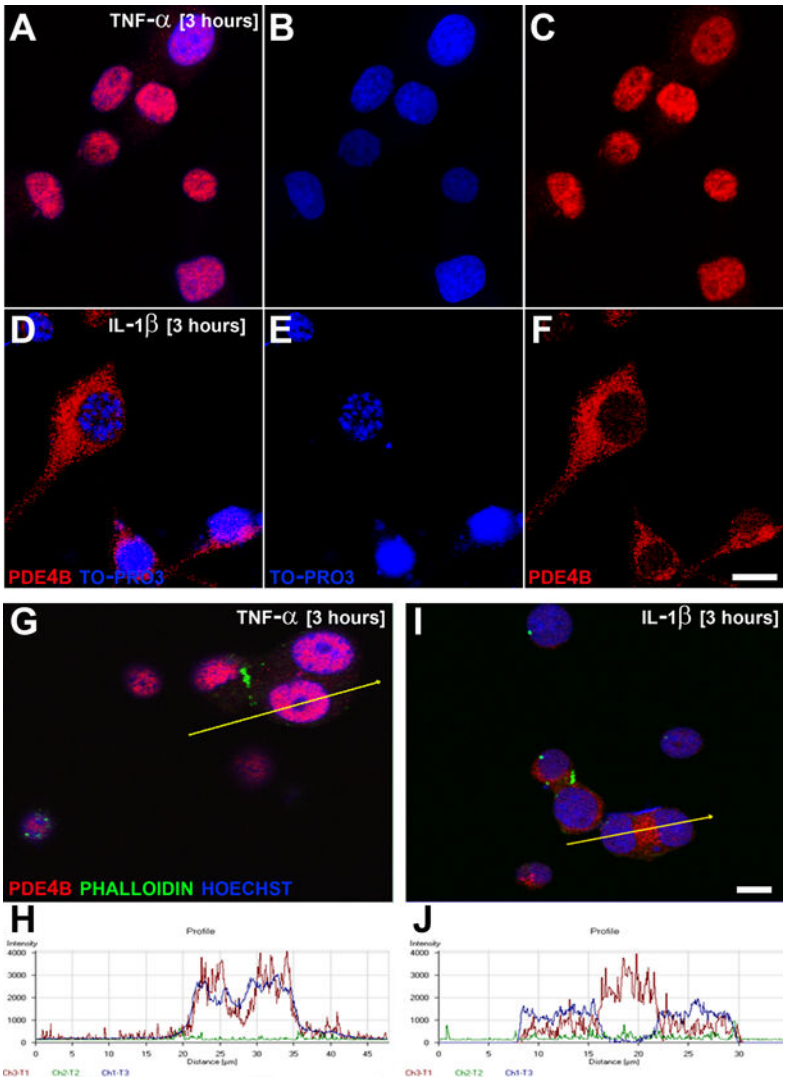

Figure 6. Nuclear translocation of PDE4B occurred in EOC2 microglia after TNF-α, but not IL-1β stimulation

A–C. TNF-α exposure produced a robust translocation of PDE4B to the nucleus as evidenced by pronounced PDE4B immunoreactivity in microglia nuclei (**C**) at 3h after stimulation **D–F.** In contrast, PDE4B immunoreactivity was confined to the cytoplasm of microglia (**F**) at 3h following IL-1β. Histogram analysis of 0.5 μm-thick sections under confocal microscopy clearly showed the nuclear (**G–H**) or cytoplasmic (**I–J**) staining of PDE4B in microglia at 3h after TNF-α or IL-1β stimulation, respectively. Results shown are the averages from 3 independent culture plate replicates for each treatment examined. All cultures were stained with TO-PRO3 or Hoechst to identify cell nuclei. Scale bars = 15μm and 10μm.

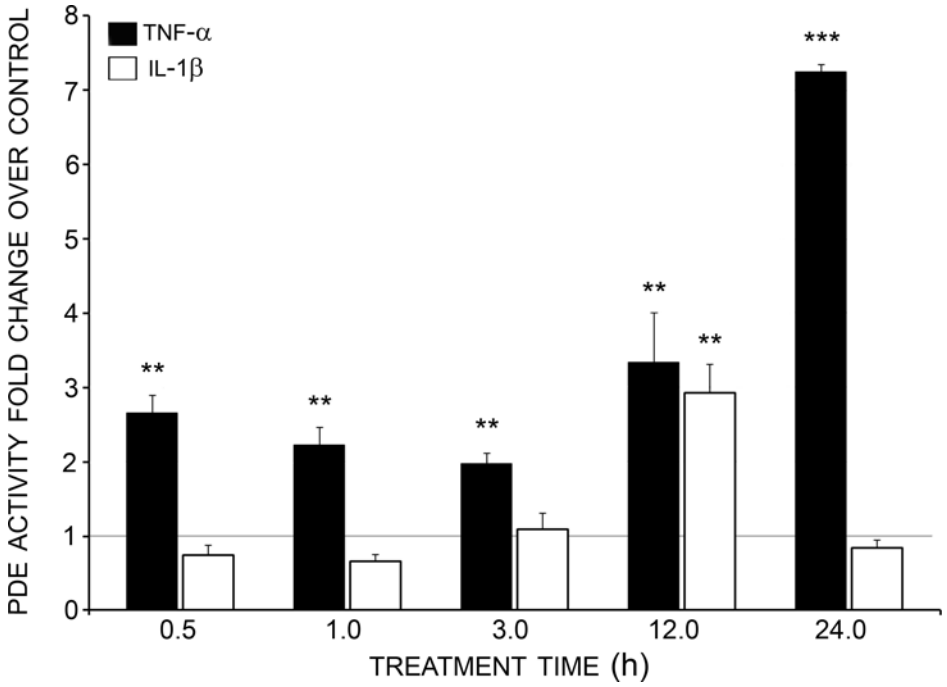

Figure 7. Total cyclic AMP dependent PDE activity increased in EOC2 microglia, being rapid and persistent with TNF-α but delayed and transient after IL-1β

TNF-α acutely increased cyclic AMP-dependent PDE activity in microglia within 30min of stimulation; activity remained significantly elevated at all time points examined and peaked at 24h. IL-1β produced only a transient increase in cyclic AMP dependent PDE activity at 12h after stimulation. Cyclic AMP-dependent PDE activity is expressed as a –fold change over naïve controls. Results shown are the averages from 4 independent culture plate replicates for each treatment and time point examined. Errors are given as SEMs. Statistical significance to naïve controls is indicated at **$p<0.01$ and ***$p<0.001$.

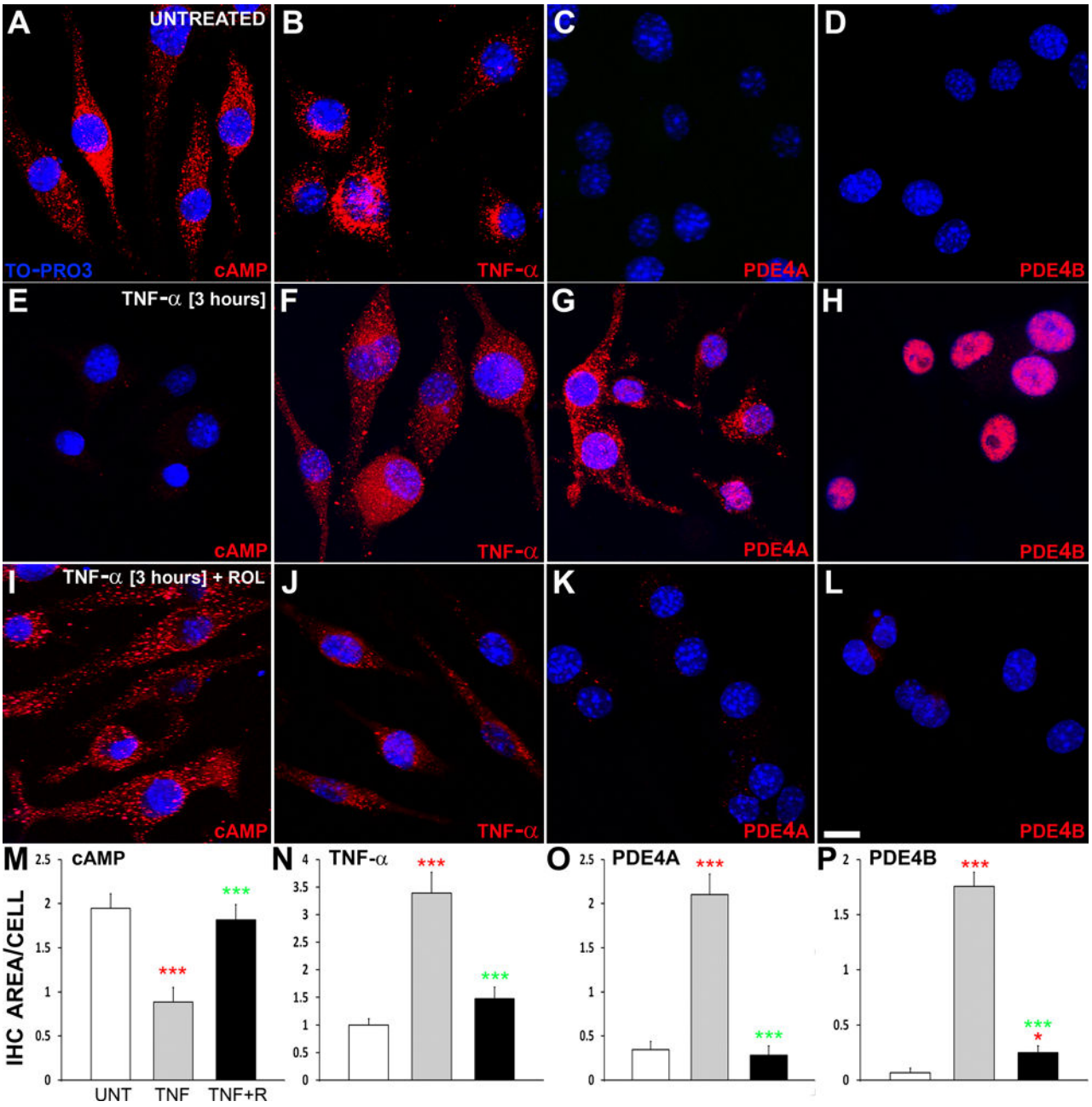

Figure 8. Rolipram prevented cyclic AMP loss and abrogated increased TNF-α, PDE4A and 4B in EOC2 microglia following TNF-α stimulation

A–D. Naïve microglia exhibited high levels of cyclic AMP, cytoplasmic (likely vesicular) TNF-α immunoreactivity but negligible levels of PDE4A and 4B. **E–H.** TNF-α stimulation produced a dramatic loss in cyclic AMP, elevated TNF-α production as well as increased PDE4A and 4B at 3h. **I–L.** Simultaneous application of Rolipram with TNF-α application abated the loss of cyclic AMP and prevented increases in TNF-α, PDE4A and 4B. **M–P.** Quantification of protein levels (by area of immunoreactivity per cell) shows changes in cyclic AMP (**M**), TNF-α (**N**), PDE4A (**O**) and PDE4B (**P**) among conditions. Results shown are the averages from 4 independent culture plate replicates for each treatment examined.

All cultures were stained with Hoechst to identify cell nuclei. Statistical significance to naïve controls is indicated at *p<0.05 and ***p<0.001 or ***p<0.001 versus TNF-α stimulated cultures. Scale bars = 15μm.

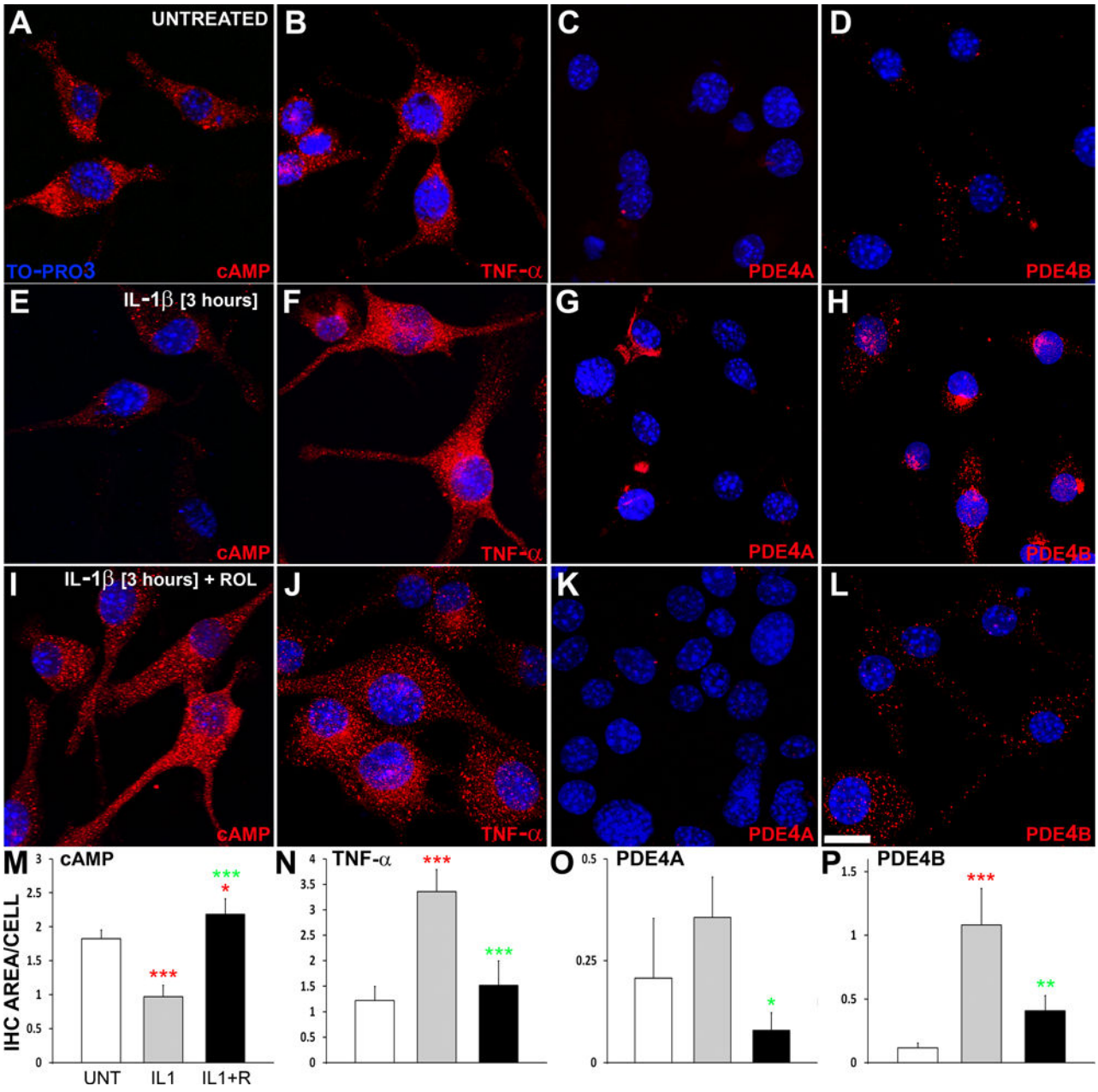

Figure 9. Rolipram prevented cyclic AMP loss and prevented increases in TNF-α, PDE4A and B in EOC2 microglia following IL-1β stimulation

A–D. Cyclic AMP, TNF-α, PDE4A and B immunoreactivity in naïve microglia. **E–H.** IL-1β stimulation produced a dramatic loss in cyclic AMP, elevated TNF-α production as well as increased PDE4B in microglia within 3h of exposure. **I–L.** Simultaneous application of Rolipram with IL-1β application abated the loss of cyclic AMP, prevented increases in TNF-α and PDE4B and reduced PDE4A. **M–P.** Quantification of protein levels (by area of immunoreactivity per cell) shows changes in cyclic AMP (**M**), TNF-α (**N**), PDE4A (**O**) and PDE4B (**P**) among conditions. Results shown are the averages from 4 independent culture plate replicates for each treatment examined. All cultures were stained with Hoechst to identify cell nuclei. Statistical significance to naïve controls is indicated at *p<0.05 and

***p<0.001 or *p<0.05, **p<0.01 and ***p<0.001 versus IL-1β stimulated cultures. Scale bars = 15μm.

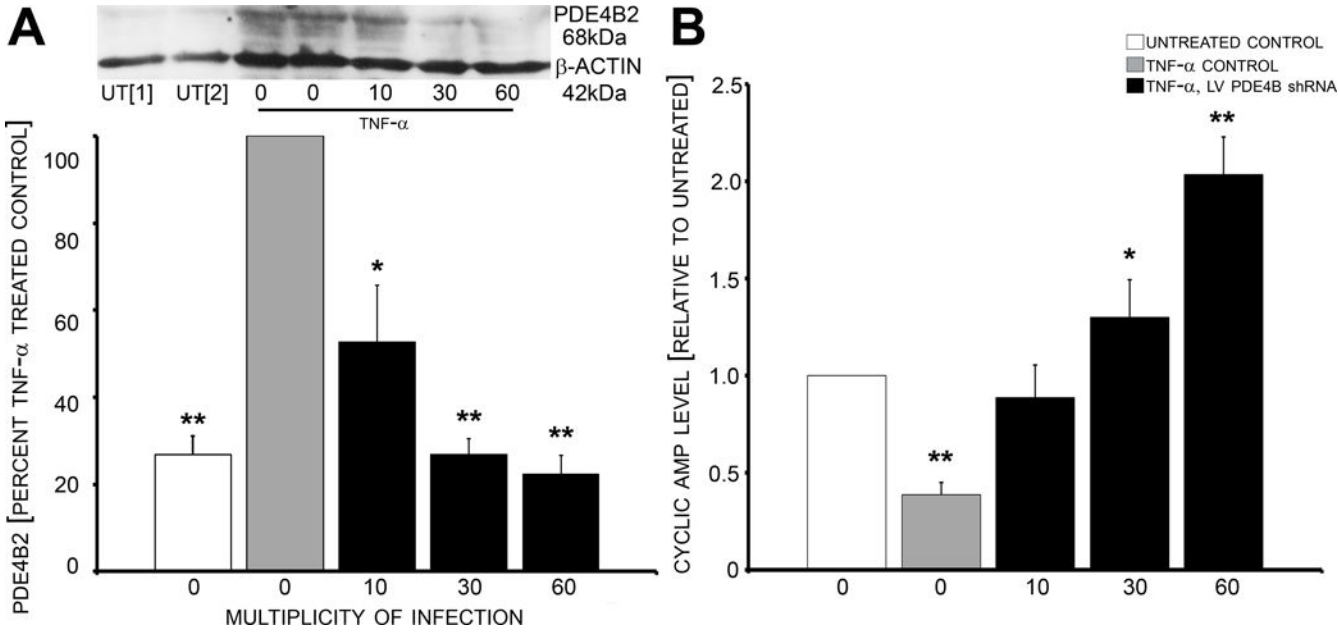

Figure 10. Lentiviral vector delivery of LV-PDE4B-shRNA reduced TNF-α-induced PDE4B2 increases and reversed cyclic AMP decreases in EOC2 microglia

A. Pre-infection of microglia for 48h with different LV-*pde4b*-shRNA MOIs prevented TNF-α-induced increases in PDE4B2 at 1h post-stimulation compared to un-infected, TNF-α-treated controls. A MOI ≥30 was most effective. **B.** LV-*pde4b*-shRNA (MOIs 10 and 30) in the same paradigm also completely reversed TNF-α-induced reductions in cyclic AMP levels. When employed at a MOI of 60, LV- *pde4b*-shRNA not only reversed but significantly increased cyclic AMP levels over that of naïve microglia controls. PDE4B2 protein and cyclic AMP levels are expressed as a percent of naïve microglia controls. PDE4B2 densitometry values were normalized to β–actin to control for protein loading after 30μg of protein was run per lane. Results shown are the averages from 3 independent culture plate replicates for each treatment examined. Errors are given as SEMs. Statistical significance to naïve controls is indicated at *$p<0.05$ and **$p<0.01$.

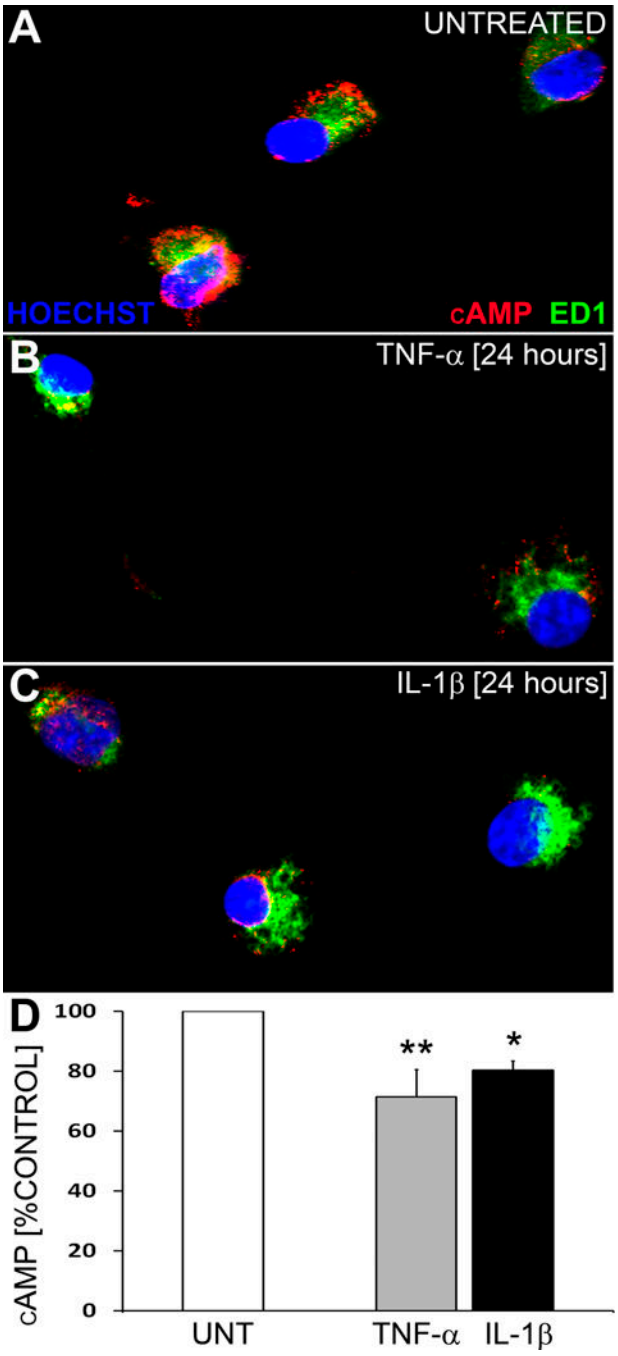

Figure 11. Exposure of adult cortex-derived microglia to pro-inflammatory cytokines reduces cyclic AMP levels

A. Primary microglia, expressing ED1, show modest levels of cyclic AMP immunoreactivity. When challenged with either TNF-α (**B**) or IL-1β (**C**), there is a significant reduction in cyclic AMP at 24h after stimulation. **D.** Quantification of cyclic AMP levels after cytokine challenge. Results shown are the averages from 3 independent culture plate replicates for each treatment examined. Cultures were stained with Hoechst to

identify cell nuclei. Errors are given as SEMs. Statistical significance to naïve controls is indicated at *$p<0.05$ and **$p<0.01$. Scale bar = 8μm.

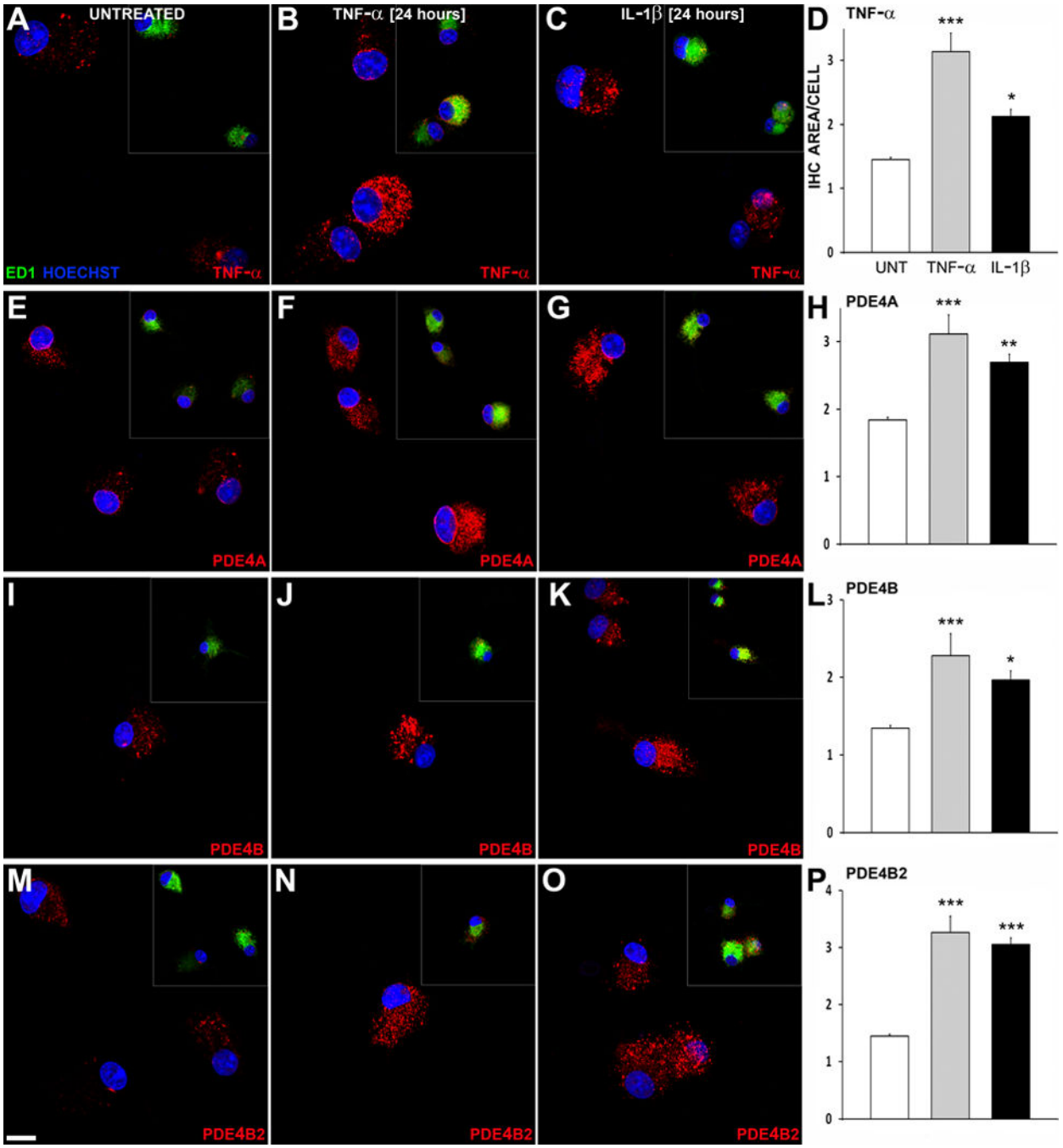

Figure 12. Increased TNF-α, as well as PDE4A, B and B2, are observed in primary microglia 24h following either TNF-α or IL-1β stimulation

A–C. TNF-α immunoreactivity is increased in TNF-α (**B**) and IL-1β (**C**) stimulated primary microglia compared to naïve controls (**A**). **E–J.** Levels of PDE4A and 4B are increased in primary microglia upon stimulation with TNF-α (**F** and **I**) and IL-1β (**G** and **J**) compared to naïve controls (**E** and **K**). **M–O.** Specifically, PDE4B2 levels are significantly enhanced in primary microglia following exposure to TNF-α (**N**) and IL-1β (**O**) compared to naïve controls (**M**). Quantification of protein levels (by area of immunoreactivity per cell) shows

changes in TNF-α (**D**), PDE4A (**H**), PDE4B (**L**) and PDE4B2 (**P**) among conditions. Results shown are the averages from 4 independent culture plate replicates for each treatment examined. Cultures were stained with Hoechst to identify cell nuclei. Image insets show ED1 immunoreactivity for the lettered region. Errors are given as SEMs. Statistical significance to naïve controls is indicated at *p<0.05, **p<0.01 and ***p<0.001. Scale bar = 10μm.

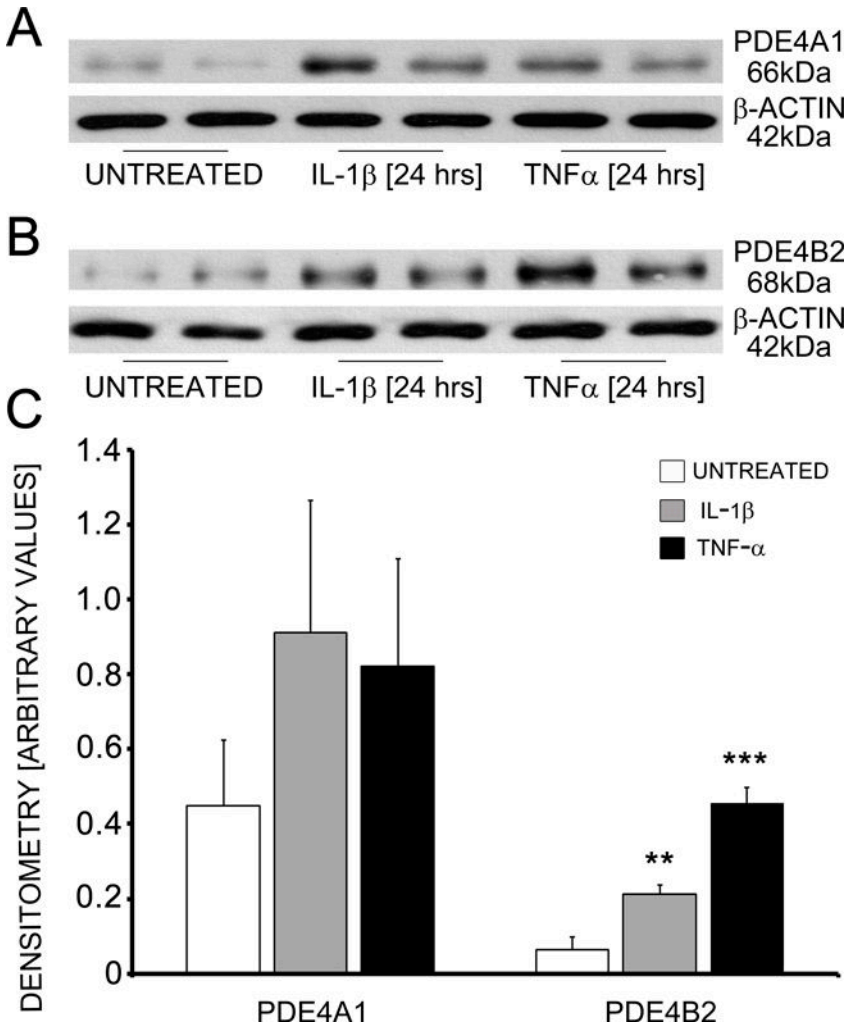

Figure 13. Both TNF-α and IL-1β increase the levels of PDE4B2 in primary microglia

A–B. Although PDE4A1 (**A**; observed MW of ~66kDa) showed a trend towards enhancement with TNF-α and IL-1β stimulation, significant increases were only observed with PDE4B2 (**B**; observed MW of ~68kDa) in primary microglia compared to naïve controls. **C.** Quantification of PDE4A1 and B2 levels using immunoblot densitometry values (arbitrary units) normalized to β-actin. Results shown are the averages from 4 independent culture plate replicates for each treatment condition; two replicates are presented on the blots in **A** and **B**. Errors are given as SEMs. Statistical significance to naïve controls is indicated at *$p<0.05$ and **$p<0.01$.

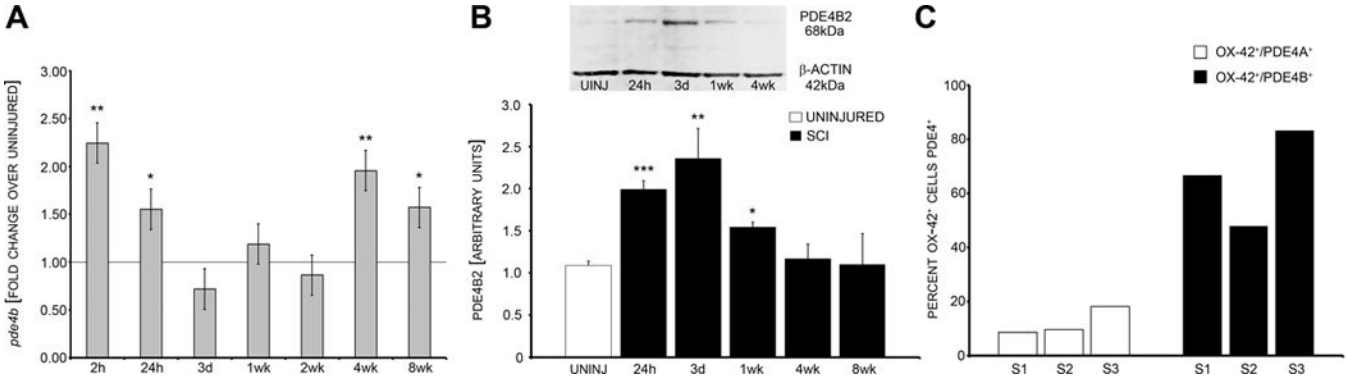

Figure 14. Increased PDE4B2 mRNA and protein are observed following acute SCI during the peak of microglial cell activation, particularly within OX-42+ cells

A. A biphasic increase in *pde4b* mRNA is observed after contusive SCI from 2–24h and at 4–8wk. The line at 1.0 indicates the average expression level of uninjured controls with temporal SCI data expressed as a –fold change over uninjured levels. **B.** PDE4B2 is significantly increased after SCI from 24h to 1wk compared to uninjured controls. **C.** Flow cytometry analysis of $PDE4^+/OX\text{-}42^+$ cells within three samples (S1–3) of the injured spinal cord at 3d after SCI shows that the majority of $OX\text{-}42^+$ microglia-macrophages express PDE4B while only a small population is $PDE4A^+$. Results shown are the averages from 5 animals for each time point examined. Errors are given as SEMs. Statistical significance to naïve controls is indicated at *p<0.05, **p<0.01 and ***p<0.001.

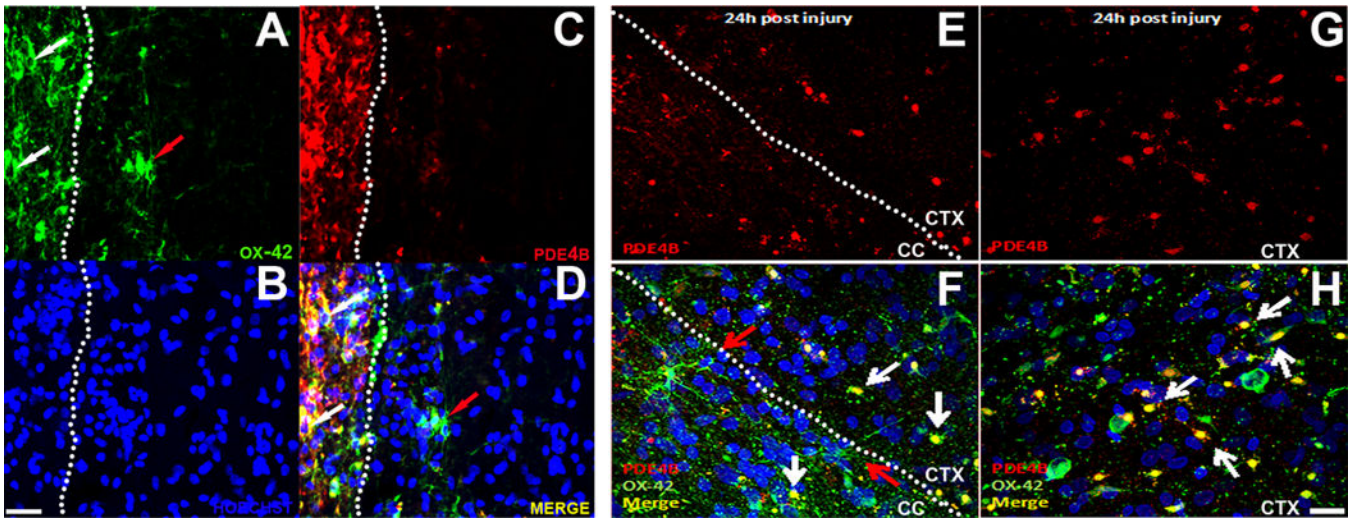

Figure 15. PDE4B is expressed in activated, but not resting, microglia acutely following CNS injury (SCI and TBI)

A–D. In OX-42^{+}/Hoechst^{+} microglia-macrophages (**A–B**) located within the injury site at 24h following contusive SCI there is pronounced PDE4B immunoreactivity (**C–D**; white arrows indicate cells that are OX-42^{+}/PDE4B^{+}). OX-42^{+} microglia located outside of the immediate injury site that exhibited a stellate morphology, characteristic of resting microglia, had no PDE4B immunoreactivity (red arrows). White dotted lines on panels A–D indicate the border of the injury epicenter. Scale bar = 40 μm. **E–H.** Similar to SCI, fluid percussion TBI led to extensive PDE4B immunoreactivity within OX-42^{+} microglia-macrophages in both white matter (**A–B**; corpus callosum, CC) and gray matter (**C–D**; parietal cortex, CTX) regions at 24h following trauma (white arrows indicate cells that are OX-42^{+}/PDE4B^{+}, white dotted line delineates the border between white and gray matter). Stellate microglia and foamy macrophages did not exhibit PDE4B immunoreactivity (red arrows). Sections were stained with Hoechst to identify cell nuclei. Scale bar = 40μm.